Available online at www.sciencedirect.com
ScienceDirect
Journal of Computational Physics 218 (2006) 159–199
JOURNAL OF COMPUTATIONAL PHYSICS
www.elsevier.com/locate/jcp

Residual distribution schemes for advection and advection–diffusion problems on quadrilateral cells ☆

P. De Palma, G. Pascazio *, D.T. Rubino, M. Napolitano

Dipartimento di Ingegneria Meccanica e Gestionale, Centro di Eccellenza in Meccanica Computazionale, Politecnico di Bari, Via Re David 200, 70125 Bari, Italy

Received 25 March 2005; received in revised form 1 February 2006; accepted 2 February 2006
Available online 22 March 2006

Abstract

This paper provides a study of some difficulties arising when extending residual distribution schemes for scalar advection and advection–diffusion problems from triangular grids to quadrilateral ones. The Fourier and truncation error analyses on a structured mesh are employed and a generalized modified wavenumber is defined, which provides a general framework for the multidimensional analysis and comparison of different schemes. It is shown that, for the advection equation, linearity preserving schemes for quadrilaterals provide lower dissipation with respect to their triangle-based counterparts and very low or no damping for high frequency Fourier modes on structured grids; therefore, they require an additional artificial dissipation term for damping marginally stable modes in order to be employed with success for pure advection problems. In the case of advection–diffusion problems, a hybrid approach using an upwind residual distribution scheme for the convective fluctuation and any other scheme for the diffusion term is only first-order accurate. On the other hand, distributing the entire residual by an upwind scheme provides second-order accuracy; however, such an approach is unstable for diffusion dominated problems, since residual distribution schemes are characterized by undamped modes associated with the discretization of the diffusive fluctuation. The present analysis allows one to determine the conditions for a stable hybrid approach to be second-order accurate and to design an optimal scheme having minimum dispersion error on a nine-point stencil. Well-documented test-cases for advection and advection–diffusion problems are used to compare the accuracy properties of several schemes.

Keywords: Residual distribution schemes; Steady scalar conservation law; Fourier analysis; Truncation error analysis

1. Introduction

Genuinely multidimensional methods, known as *Residual Distribution* ($\mathcal{RD}$) or *Fluctuation Splitting* ($\mathcal{FS}$) schemes, have been successfully developed by different research groups and have become an attractive

☆ This research has been supported by the MIUR and the Politecnico di Bari, grant CofinLab 2000 (CEMeC). The authors are grateful to the reviewers for their precious suggestions.
* Corresponding author.
E-mail addresses: depalma@poliba.it (P. De Palma), pascazio@poliba.it (G. Pascazio), dt.rubino@poliba.it (D.T. Rubino), napolita@poliba.it (M. Napolitano).

0021-9991/$ - see front matter © 2006 Elsevier Inc. All rights reserved.
doi:10.1016/j.jcp.2006.02.003

alternative to Finite Volume and Finite Element ($\mathcal{FE}$) methods for discretizing advection and advection–diffusion problems on unstructured triangular grids [1–9]. On the other hand, $\mathcal{RD}$ methods for quadrilateral grids, which, for example, are the optimal choice for discretizing boundary layer regions, have not yet reached the same level of maturity and reliability. This paper aims at understanding the causes and possibly remove them. The origin of residual distribution methods for quadrilateral cells can be traced back to the work of Ni [10], who proposed a Lax–Wendroff-type scheme with second-order accuracy in space and time. Then, several upwind schemes have been designed, such as the ones provided in [11,12], where the residual is distributed to downstream nodes with respect to the advection velocity. Furthermore, the $\mathcal{RD}$ schemes successfully developed for triangular cells, such as the N, LDA, LW, and PSI schemes, have been extended to cell-vertex quadrilateral grids in [13]. More recently, a method has been proposed to apply the $\mathcal{RD}$ schemes to arbitrary conservation laws [14] and finite elements [15] in the absence of a conservative linearization [16]. In spite of these efforts, it is the authors opinion that a thorough analysis of the accuracy and stability properties of $\mathcal{RD}$ schemes on rectangular grids is still lacking and is worth pursuing. Therefore, this work addresses some issues arising when extending $\mathcal{RD}$ schemes for scalar advection and advection–diffusion problems from triangular grids to quadrilateral ones. The study is performed using the Fourier and truncation error analyses on a structured mesh, in order to provide a strategy for the design of second-order accurate stable schemes. In particular, the spectral analysis presented in this paper is multidimensional in the sense that it is not restricted to the case of Fourier modes aligned with the advection velocity, as done for example in [17–19], and all of the grid-resolved two-dimensional wavenumbers are analyzed for a given advection angle.

Cell-vertex $\mathcal{RD}$ schemes are based on two main steps: (i) evaluating the fluctuation, namely, the flux balance over the cell; (ii) distributing the fluctuation to its vertices.

Concerning the advection term, the cell residual is evaluated using a contour integral of the flux along the cell faces, which assumes a linear reconstruction of the unknown and thus avoids the need for a conservative linearization. For the distribution step, the linearity preserving LDA and LW schemes [13] have been used as a starting point. It is noteworthy that for the case of scalar advection the extension to Cartesian grids of the LW scheme for triangles recovers Ni's scheme [10]. Then, a conservative $SUPG$ method for quadrilateral cells is derived and, finally, a dissipation-free minimum-dispersion-error second-order accurate scheme is provided. The Fourier analysis shows that linearity preserving ($\mathcal{LP}$) schemes, when applied to quadrilateral cells, are marginally stable, thus requiring an additional numerical dissipation to compute advection problems. In this paper, $\mathcal{LP}$ schemes are effectively stabilized by the addition of the bias term of the $SUPG$ scheme, without affecting their order of accuracy.

The diffusion term is evaluated either by a standard Galerkin $\mathcal{FE}$ scheme or by a residual based approach. In the latter case, the diffusive fluctuation is evaluated by a contour integral, whereby the gradients at the nodes are computed by a Green–Gauss reconstruction. For the distribution of the diffusive fluctuation, two alternatives have been discussed using either an upwind or a centred scheme.

A thorough analysis of second-order accurate discretizations of the advection–diffusion equation is then provided.

Finally, the theoretical findings are validated by a series of numerical experiments carried out for advection and advection–diffusion problems.

2. Model problem and $\mathcal{RD}$ schemes

2.1. Model equation

Consider the two-dimensional scalar conservation law with a dissipative term:

$$\begin{aligned} &\frac{\partial u}{\partial t} + \nabla \cdot \mathbf{f} = \mu \nabla^2 u, \\ &\text{with} \quad u : \Omega \times [0, +\infty[\to \mathbb{R}, \Omega \subseteq \mathbb{R}^2, \quad \mathbf{f} = (f(u), g(u))^{\mathcal{T}}. \end{aligned} \tag{1}$$

For linear advection, the flux vector can be expressed as $\mathbf{f} = \boldsymbol{\lambda} u$, where $\boldsymbol{\lambda} = (a, b)^{\mathcal{T}}$ is the advection velocity, whereas, for Burgers' non-linear equation, the flux vector is given by $\mathbf{f} = (u^2/2, u)^{\mathcal{T}}$. For a divergence-free

advection velocity, Eq. (1) reduces to the scalar advection–diffusion equation. Pure convection and pure diffusion are obtained when the coefficient μ or the flux vector $\mathbf{f}$ are equal to zero, respectively. Eq. (1) is discretized on a computational domain, Ω, divided into triangular or quadrilateral elements, Ω_E, the generic node being labeled i.

2.2. Basics of the $\mathcal{RD}$ approach

Cell-vertex $\mathcal{RD}$ schemes are based on two main steps: (i) evaluating the residual over each element; (ii) splitting the residual into contributions (signals) to be assigned to the vertices of the cell. The first step applies to both the residual due to the advection term, namely, the inviscid flux balance over the element,

$$\phi^{E,a} = \int_{\Omega_E} \nabla \cdot \mathbf{f}_h \, \mathrm{d}\Omega, \tag{2}$$

and the residual due to the diffusion one,

$$\phi^{E,d} = \int_{\Omega_E} \mu \nabla^2 u_h \, \mathrm{d}\Omega. \tag{3}$$

In the equations above, u_h is the continuous piecewise linear (for triangles) or bilinear (for quadrilaterals) approximation function; $\mathbf{f}_h$ is the corresponding numerical flux vector, which must be a continuous and differentiable approximation of $\mathbf{f}$ and must converge locally to $\mathbf{f}$. It is noteworthy that the evaluation of $\nabla^2 u_h$ on linear and bilinear elements using only the nodal values for each element is meaningless (in the case of triangular linear elements $\nabla u_h = \text{const.}$ and $\phi^{E,d} = 0$ over each element). Therefore, the discrete Laplacian operator is defined on a non-compact stencil using the nodal values of the neighboring elements, as described in Section 2.4.2. Alternatively, a weighted residual approach has been employed as described in Section 2.4.1. The second step is performed using suitable distribution coefficients for the advective and the diffusive fluctuations, respectively:

$$\phi_j^{E,a} = \gamma_j^E \phi^{E,a}, \quad \phi_j^{E,d} = \alpha_j^E \phi^{E,d}, \tag{4}$$

where γ_j^E and α_j^E are the distribution coefficients of element Ω_E to node j, and $\phi_j^{E,a}$ and $\phi_j^{E,d}$ are the corresponding signals assigned to it. Needless to say, the distribution coefficients sum up to one within each element, for conservation:

$$\sum_{j \in E} \gamma_j^E = 1, \quad \sum_{j \in E} \alpha_j^E = 1.$$

Finally, the solution at each node is updated by summing up the contributions coming from all elements surrounding it. Since only *steady-state* solutions are of interest in this work, a simple mass lumping of the weak form of Eq. (1) provides the following semi-discrete formula to update the solution:

$$|\Omega_i| \frac{\mathrm{d}u_i}{\mathrm{d}t} = -\sum_{\Omega_E \in \Delta_i} \phi_i^{E,a} + \sum_{\Omega_E \in \Delta_i} \phi_i^{E,d}, \tag{5}$$

where $|\Omega_i|$ indicates the area of the median dual cell of node i and Δ_i represents the set of elements sharing node i. In this work, Eq. (5) is integrated in time by the Euler explicit scheme, using local time-stepping to accelerate convergence to steady state. In the following, the discretization of the advection term will be considered at first, using several linear and non-linear $\mathcal{RD}$ schemes, the superscript "a" being omitted, for brevity; then, the diffusion term will be considered.

2.3. $\mathcal{RD}$ schemes for the advection term

The fluctuation is computed as the flux balance over the cell,

$$\phi^E = \int_{\Omega_E} \nabla \cdot \mathbf{f}_h \, \mathrm{d}\Omega = \oint_{\partial\Omega_E} \mathbf{f}_h \cdot \mathbf{n} \, \mathrm{d}\ell. \tag{6}$$

For triangular elements, due to the linear variation of u_h over each element, the fluctuation can be computed, exactly, as

$$\phi^E = \sum_{j\in E} k_j u_j, \quad k_j = \frac{1}{2}\boldsymbol{\lambda}\cdot\mathbf{n}_j, \tag{7}$$

where k_j is the inflow parameter of node j and $\mathbf{n}_j$ is the inward unit vector normal to the edge opposing node j, multiplied by the length of the edge itself (see Fig. 1(a)). In the case of non-linear advection, $\boldsymbol{\lambda}$ is a cell-linearized advection velocity which guarantees conservation, see [3], for more details.

For quadrilateral elements, in the absence of a conservative linearization, the fluctuation is computed by the contour integral of the fluxes in Eq. (6) using the three point Simpson rule on each edge. Notice that the bilinear (Q1) reconstruction of the unknown, u_h, assuming standard Lagrangian bilinear shape functions mapped from the biunit element onto the physical one, guarantees that the unknown is linear along the edges of the element. The inflow parameter k_j is still given by the definition (7), $\mathbf{n}_j$ being the unit vector normal to the diagonal opposite to node j multiplied by the diagonal length, as shown in Fig. 1(b).

2.3.1. Linearity preserving linear schemes

Linearity preserving ($\mathcal{LP}$) schemes are characterized by bounded distribution coefficients, so that the signals (and the solution update) vanish as the fluctuation vanishes:

$$\lim_{\phi^E\to 0}\phi_j^E = \lim_{\phi^E\to 0}\gamma_j^E\phi^E = 0. \tag{8}$$

For pure advection problems, Abgrall [7] proved that second-order space accuracy at steady state is equivalent to require that $\phi_j^E = \mathcal{O}(h^3)$. Since the linear representation of the solution on $P1$ and $Q1$ elements guarantees that $\phi^E = \mathcal{O}(h^3)$ and the distribution coefficients γ_j^E are bounded, it follows that the $\mathcal{LP}$ property ensures second-order accuracy. In the following, two linear $\mathcal{LP}$ schemes are described, namely, the *LDA* and Lax–Wendroff (*LW*) ones [1,3].

The *LDA* scheme is defined by the following distribution coefficients:

$$\gamma_i^{LDA} = k_i^+\left(\sum_{j\in E} k_j^+\right)^{-1}, \tag{9}$$

where $k_i^+ = \max(0, k_i)$. This is a *multidimensional upwind* scheme, in the sense that no signal is sent to upwind nodes ($k_i \leqslant 0 \Rightarrow \gamma_i^{LDA} = 0$). Notice that, in the case of quadrilateral cells, this scheme is two-target except when $\boldsymbol{\lambda}$ is aligned with one of the diagonals, in which case it becomes one-target, see Fig. 1(b). It is noteworthy that, for quadrilateral elements, the distribution step provided in Eq. (9) is equivalent to the one proposed in [11].

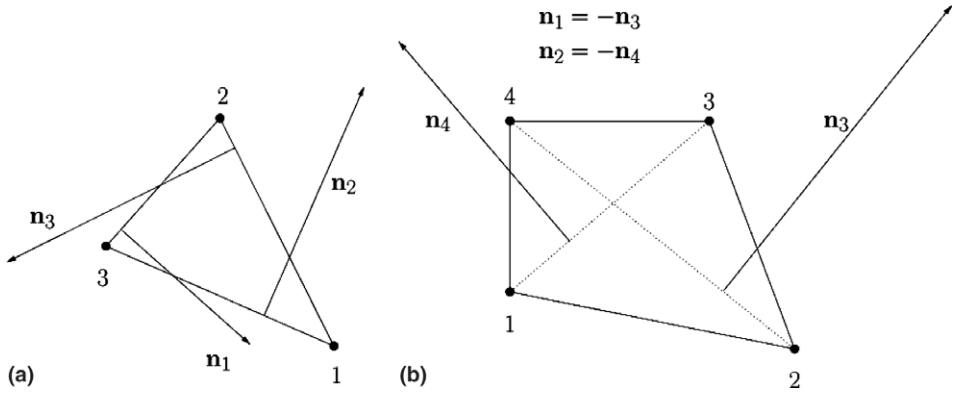

Fig. 1. Normals for the definition of the inflow parameters.

The LW scheme is characterized by the following distribution coefficients:

$$\gamma_i^{LW} = \frac{1}{e} + \frac{k_i \Delta t}{2|\Omega_E|}, \tag{10}$$

where Δt is the time-step, $|\Omega_E|$ is the element area, and e is the number of nodes per element. For the case of a uniform Cartesian mesh, this scheme coincides with Ni's Lax–Wendroff scheme [10].

2.3.2. The N scheme

The conservative formulation of the N scheme presented in [14] is used, which has already been applied to quadrilaterals for the solution of the Euler equations [15]. The scheme is first-order accurate and is defined as

$$\phi_i^N = k_i^+(u_i - u_c), \quad u_c = \left(\sum_{j\in E} k_j^+\right)^{-1}\left[\left(\sum_{j\in E} k_j^+ u_j\right) - \phi^E\right], \tag{11}$$

where u_c allows to satisfy conservation regardless of the linearization used. Such a scheme, unlike the standard one for triangular grids [1], has not been proven to be positive. Nonetheless, it is very robust and yields oscillation-free solutions.

2.3.3. The non-linear PSI scheme

According to Godunov's theorem, a linear scheme cannot be both positive and linearity preserving. A common way to obtain a monotone $\mathcal{LP}$ scheme is to limit the coefficients of a positive linear scheme. The *PSI* scheme is based on the use of the *minmod* limiter applied to the distribution coefficients of the N scheme [3], namely:

$$\gamma_i^{PSI} = \frac{(\gamma_i^N)^+}{\sum_{j\in E}(\gamma_j^N)^+}, \tag{12}$$

where

$$\gamma_j^N = \frac{\phi_j^N}{\phi^E} \quad \text{and} \quad (\gamma_j^N)^+ = \max(0, \gamma_j^N). \tag{13}$$

2.3.4. The SUPG scheme

The $\mathcal{FE}$ Streamline Upwind Petrov–Galerkin (*SUPG*) method, originally introduced by Brooks and Hughes [20], can be recast into the present $\mathcal{RD}$ framework, as follows.

The signal to node i obtained using the standard *SUPG* formulation reads

$$\phi_i^{E,SUPG} = \int_{\Omega_E} \omega_i \nabla \cdot \mathbf{f}_h \, \mathrm{d}\Omega, \tag{14}$$

the weight function being defined as

$$\omega_i = N_i + \tau(\boldsymbol{\lambda} \cdot \nabla N_i),$$

where N_i are the standard Lagrangian shape functions and $\tau = h/(2\|\boldsymbol{\lambda}\|)$, see [3] for details.

In the case of triangular cells, where the $P1$ Lagrangian shape functions are linear, the upwind bias is constant over each element and the distribution coefficients can be easily evaluated as

$$\gamma_i^{SUPG} = \frac{1}{3} + \tau \frac{k_i}{|\Omega_E|}. \tag{15}$$

In the case of quadrilateral cells, the Lagrangian shape functions are defined on the biunit (master) $Q1$ element and mapped onto the physical one, see Fig. 2. Since the upwind bias added to the $Q1$ Lagrangian shape functions is not constant over the element, a numerical quadrature of the integral in Eq. (14) is needed, which has to fulfill the following relation:

$$\phi^E = \sum_{i\in E} \phi_i^E = \oint_{\partial\Omega_E} \mathbf{f}_h \cdot \mathbf{n} \, \mathrm{d}\ell, \tag{16}$$

to maintain conservation at the discrete level.

Remark 1. *Conservation is fulfilled by integrating the right-hand side of Eq. (14) as follows*:

$$\phi_i^{E,SUPG} = \oint_{\partial\Omega_E} N_i \mathbf{f}_h \cdot \mathbf{n}\,\mathrm{d}\ell - \int_{\Omega_E} \mathbf{f}_h \cdot \nabla N_i\,\mathrm{d}\Omega + \int_{\Omega_E} \tau(\boldsymbol{\lambda}\cdot\nabla N_i)\nabla\cdot\mathbf{f}_h\,\mathrm{d}\Omega. \tag{17}$$

Proof. Summing up all signals in an element, one obtains

$$\begin{aligned}\sum_{i\in E}\phi_i^{E,SUPG} &= \sum_{i\in E}\oint_{\partial\Omega_E} N_i\mathbf{f}_h\cdot\mathbf{n}\,\mathrm{d}\ell - \sum_{i\in E}\int_{\Omega_E}\mathbf{f}_h\cdot\nabla N_i\,\mathrm{d}\Omega + \sum_{i\in E}\int_{\Omega_E}\tau(\boldsymbol{\lambda}\cdot\nabla N_i)\nabla\cdot\mathbf{f}_h\,\mathrm{d}\Omega \\ &= \oint_{\partial\Omega_E}\sum_{i\in E} N_i\mathbf{f}_h\cdot\mathbf{n}\,\mathrm{d}\ell - \int_{\Omega_E}\mathbf{f}_h\cdot\sum_{i\in E}\nabla N_i\,\mathrm{d}\Omega + \int_{\Omega_E}(\tau\boldsymbol{\lambda}\cdot\sum_{i\in E}\nabla N_i)\nabla\cdot\mathbf{f}_h\,\mathrm{d}\Omega.\end{aligned} \tag{18}$$

Standard Lagrangian shape functions obey to constant summation and conservation constraints:

$$\sum_{i\in E} N_i(\mathbf{x}) = 1; \quad \sum_{i\in E}\nabla N_i(\mathbf{x}) = 0; \qquad \forall \mathbf{x}\in\Omega_E. \tag{19}$$

Therefore, the first term in the right-hand side of Eq. (18) coincides with the right-hand side of Eq. (16) and the remaining terms are identically zero. □

From a practical point of view, when evaluating the signal to node i, the contour integral in Eq. (17) is computed using the Simpson rule along each edge, whereas the area integrals are computed using the Gauss quadrature rule with four base points per element, provided that an average value of $\boldsymbol{\lambda}$ is computed for the case of non-linear advection.

The scheme of Eq. (17) can be considered an $\mathcal{FE}$ Galerkin scheme modified by an additional bias and is second-order accurate on non Cartesian grids. In previous works by the authors, see e.g. [21], where integration by parts was applied also to the bias term, only first-order accurate solutions were obtained.

2.4. Discretization of the diffusion term

2.4.1. The $\mathcal{FE}$ Galerkin approach

In the $\mathcal{RD}$ framework [3–5], the standard $\mathcal{FE}$ Galerkin method [22] is usually employed to discretize the diffusion term. For the internal nodes, using a weighted residual formulation with $\omega_i = N_i$, one has

$$\begin{aligned}\int_\Omega \omega_i\mu\nabla^2 u_h\,\mathrm{d}\Omega &= \int_\Omega N_i\mu\nabla^2 u_h\,\mathrm{d}\Omega = \underbrace{\oint_{\partial\Omega} N_i\mu\nabla u_h\cdot\mathbf{n}\,\mathrm{d}\ell}_{=0} - \int_\Omega \mu\nabla N_i\cdot\nabla u_h\,\mathrm{d}\Omega \\ &= -\sum_{\Omega_E\in\Delta_i}\int_{\Omega_E}\mu\nabla N_i\cdot\nabla u_h\,\mathrm{d}\Omega = \sum_{\Omega_E\in\Delta_i}\phi_i^{E,d},\end{aligned} \tag{20}$$

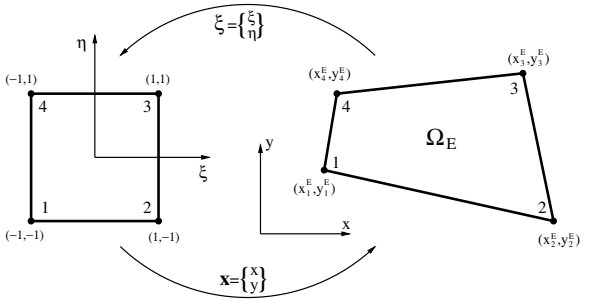

Fig. 2. Mapping from the biunit element onto the physical one.

where the underbraced term is equal to zero, the weight functions being compact. For inflow boundary nodes, Dirichlet boundary conditions are employed, no conditions being needed for outflow ones.

For $P1$ linear triangular elements, the shape function gradients are given as

$$\nabla N_i = \frac{\mathbf{n}_i}{2|\Omega_E|}. \tag{21}$$

Therefore, substituting the above expression into Eq. (20), the discretized diffusion term reads

$$\sum_{\Omega_E \in \Delta_i} \phi_i^{E,d} = -\sum_{\Omega_E \in \Delta_i} \int_{\Omega_E} \mu \frac{\mathbf{n}_i}{2|\Omega_E|} \cdot \nabla u_h \, \mathrm{d}\Omega = -\sum_{\Omega_E \in \Delta_i} \mu \frac{\mathbf{n}_i}{2} \cdot \nabla u_h, \tag{22}$$

where, keeping into account that ∇u_h is constant over the element,

$$\nabla u_h = \sum_{j \in \Omega_E} u_j \nabla N_j = \sum_{j \in \Omega_E} u_j \frac{\mathbf{n}_j}{2|\Omega_E|}. \tag{23}$$

For quadrilateral elements, the integral in Eq. (20),

$$\int_{\Omega_E} \mu \nabla N_i \cdot \nabla u_h \, \mathrm{d}\Omega, \tag{24}$$

has to be computed directly. Here, a four-point Gauss quadrature rule is employed.

2.4.2. The residual based approach

For pure diffusion problems, where there is no relevant direction in the flow, the most appropriate distribution is a centred one (i.e., $\alpha_j^E = 1/4 \ \forall j$). For advection–diffusion problems, one could choose to distribute $\phi^{E,d}$ according to the same (most probably *upwind*) coefficients chosen for the convective term, namely, $\alpha_i^E = \gamma_i^E$. In this case, the resulting schemes maintain the $\mathcal{LP}$ property, provided that γ_i^E are bounded. In fact, the analysis proposed in [7] for the advection equation can be easily extended to the case of the advection–diffusion equation by requiring that $\phi^E = \phi^{E,a} + \phi^{E,d} = \mathcal{O}(h^3)$. This condition can be fulfilled assuming second-order approximations for the advective and diffusive fluxes.

The viscous fluctuation is evaluated as a contour integral, namely,

$$\phi^{E,d} = \int_{\Omega_E} \mu \nabla^2 u_h \, \mathrm{d}\Omega = \oint_{\partial\Omega_E} \mu \nabla u_h \cdot \mathbf{n} \, \mathrm{d}\ell. \tag{25}$$

In order to ensure a second-order approximation of the diffusive flux, the solution gradient is reconstructed at the nodes by a Green–Gauss procedure, using only internal cells for boundary nodes, and then the fluctuation is computed applying the trapezoidal rule along each edge. It is worth observing that this reconstruction procedure for the nodal gradients leads to a centred second-order accurate finite difference scheme, for a uniform Cartesian grid. Furthermore, the Green–Gauss reconstruction needs a larger stencil with respect to using the $\mathcal{FE}$ Galerkin approach plus the $\mathcal{RD}$ discretization of the advective fluctuation, as already pointed out in [5].

3. Truncation error analysis

3.1. Advection equation

In this section, the truncation error analysis is carried out on a uniform structured grid, with mesh spacing h, for the case of the linear advection equation, with constant velocity $\boldsymbol{\lambda}$ inclined at an angle $\delta = \arctan(b/a)$ with respect to the horizontal direction. Without loss of generality, the reference axes are oriented in such a way that $\delta \in [0, \pi/2]$. A general analysis for two-dimensional convection operators on structured grids [23] shows that second-order accurate schemes are characterized by *zero* crosswind diffusion. Indeed, projecting the linear advection equation onto the natural coordinate system (ξ, η) aligned with $\boldsymbol{\lambda}$, one has

$$\frac{\partial u}{\partial t} + \|\boldsymbol{\lambda}\| \frac{\partial u}{\partial \xi} = 0.$$

The finite-difference expressions of several schemes of interest are provided in Appendix A.1. For $\mathcal{RD}$ schemes, these expressions are obtained writing the signals ϕ_i from each element sharing node i in terms of the values of the solution at the vertices of the element itself. Then, the truncation error is computed by a Taylor series expansion around node i. Following this procedure, the truncation errors for four schemes of interest are evaluated and discussed in the following.

The truncation error (TE) of an $\mathcal{LP}$ scheme is obtained at first, as

$$\mathrm{TE}^{\mathcal{LP}} = -\frac{1}{48} h^2 \frac{\partial^3 u}{\partial \eta^3} \|\boldsymbol{\lambda}\| \sin(4\delta) + \mathcal{O}(h^3). \tag{26}$$

It appears that:

(a) like in the case of $\mathcal{LP}$ schemes for triangular cells [3], the *crosswind diffusion*, namely, the coefficient of $\partial^2 u/\partial \eta^2$, is equal to *zero*;
(b) the leading term of $\mathrm{TE}^{\mathcal{LP}}$ has a *dispersive* character;
(c) the leading term of $\mathrm{TE}^{\mathcal{LP}}$ is proportional to $\sin(4\delta)$; the same is true for all higher order terms, so that $\mathrm{TE}^{\mathcal{LP}} = 0$ for $\boldsymbol{\lambda}$ aligned either with the grid coordinate axis or with a diagonal;
(d) the leading term of $\mathrm{TE}^{\mathcal{LP}}$ does not depend on the distribution coefficients; thus, an $\mathcal{LP}$ scheme on $Q1$ elements cannot be more than second-order accurate, the accuracy being limited by the solution reconstruction within each element.

The TE of the finite-difference second-order accurate (fully) upwind scheme is then evaluated as

$$\mathrm{TE}^{\mathcal{FD}\text{-upw2}} = \frac{1}{12} h^2 \frac{\partial^3 u}{\partial \eta^3} \|\boldsymbol{\lambda}\| \sin(4\delta) + \mathcal{O}(h^3), \tag{27}$$

which is of the same order, but four times higher, than $\mathrm{TE}^{\mathcal{LP}}$. The most accurate $\mathcal{FD}$ approximation of the convective term based on the nine-point computational molecule of Fig. 3 is then considered:

$$(\boldsymbol{\lambda} \cdot \nabla u)_i \simeq \frac{1}{12h} \{a[u_n - u_p + 4(u_m - u_q) + u_l - u_j] + b[u_n - u_l + 4(u_o - u_k) + u_p - u_j]\}, \tag{28}$$

which has the following truncation error:

$$\mathrm{TE}^{\mathcal{FD}\text{-cen4}} = \frac{\|\boldsymbol{\lambda}\|}{720} \frac{\partial^5 u}{\partial \eta^5} h^4 \sin(4\delta) + \mathcal{O}(h^6).$$

This scheme, introduced by Abarbanel and Kumar [24], has been recently recast into a residual-based framework by Lerat and Corre [25]; on a Cartesian grid, it coincides with the discretization obtained by the $\mathcal{FE}$

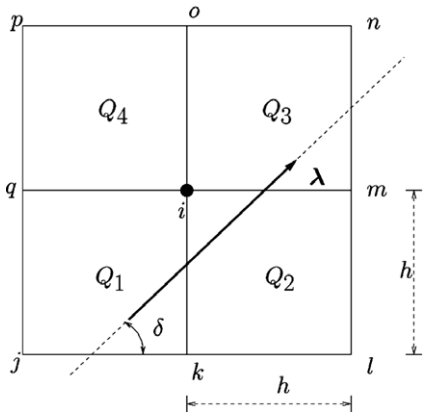

Fig. 3. Nine-point computational molecule for the truncation error analysis.

Galerkin procedure and is well known to be unstable. Finally, the TE of the *SUPG* scheme has been considered:

$$\mathrm{TE}^{SUPG} = \frac{1}{96} h^3 \frac{\partial^4 u}{\partial \eta^4} \|\boldsymbol{\lambda}\| \sin^2(2\delta) + \mathcal{O}(h^4). \tag{29}$$

It is well known that the *SUPG* scheme was designed to stabilize the $\mathcal{FE}$ Galerkin scheme for advection problems, by introducing a fourth-order cross-wind diffusion term.

3.2. Advection–diffusion equation

In this section, the truncation error analysis is carried out for the case of the linear advection–diffusion equation. The finite-difference expressions of the diffusion term are provided in Appendix A.2 for the $\mathcal{LP}$ and $\mathcal{FE}$ Galerkin ($\mathcal{FE}$-*Gal*) schemes. Here, $\mathcal{RD}$ $\mathcal{LP}$ schemes are used to discretize the advection term, in order to establish the conditions to be satisfied for second-order accuracy.

For $\mathcal{RD}$ schemes on triangular grids, Nishikawa and Roe [26] have shown that second-order accuracy can be achieved if the scheme maintains the $\mathcal{LP}$ property at a global level, namely, if the entire fluctuation is distributed using bounded coefficients. For the uniform triangulation of Fig. 4, taking into account the following relations:

$$\begin{aligned} &\gamma_1 + \gamma_3 + \gamma_5 = 1, \\ &\gamma_2 + \gamma_4 + \gamma_6 = 1, \end{aligned} \tag{30}$$

which must hold for conservation, the truncation error is obtained as

$$\mathrm{TE}^{\mathcal{LP}} = -\frac{h}{2}[(\gamma_1 - \gamma_4)\partial_x + (\gamma_2 - \gamma_5)\partial_y]r + \mathcal{O}(h^2). \tag{31}$$

Therefore, the scheme is second-order accurate at steady state, since the residual $r = -\boldsymbol{\lambda} \cdot \nabla u + \mu \nabla^2 u$ vanishes. In general, a first-order accurate solution is obtained, as for a hybrid scheme using an $\mathcal{LP}$ discretization of the advection term and the $\mathcal{FE}$-*Gal* approach for the diffusion term. Considering that the $\mathcal{FE}$-*Gal* diffusive operator is second-order accurate by itself and gives no contribution to the dissipative first-order term, the TE of such a scheme reads

$$\mathrm{TE}^{\mathcal{LP}/\mathcal{FE}\text{-}Gal} = -\frac{h}{2}[(\gamma_1 - \gamma_4)\partial_x + (\gamma_2 - \gamma_5)\partial_y]r^a + \mathcal{O}(h^2). \tag{32}$$

Since the convective residual $r^a = -\boldsymbol{\lambda} \cdot \nabla u$ does not necessarily vanish at steady state, the considered hybrid scheme is second-order accurate only for $\gamma_1 = \gamma_4$ and $\gamma_2 = \gamma_5$.

In this work, a similar analysis is carried out for quadrilateral grids, obtaining an equivalent result. For $\mathcal{LP}$ schemes and with reference to Fig. 5, the truncation error reads

$$\mathrm{TE}^{\mathcal{LP}} = -\frac{h}{2}[(\gamma_1 - \gamma_3)(\partial_x + \partial_y) - (\gamma_2 - \gamma_4)(\partial_x - \partial_y)]r + \mathcal{O}(h^2), \tag{33}$$

which provides second-order accuracy, since $r = 0$ at steady state. On the other hand, for a hybrid discretization employing an $\mathcal{LP}$ scheme plus the $\mathcal{FE}$-*Gal* approach, one has

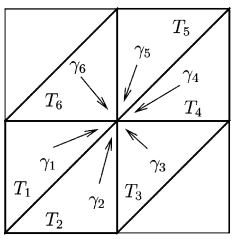

Fig. 4. Uniform triangulation.

$$\mathrm{TE}^{\mathcal{LP}/\mathcal{FE}\text{-}Gal} = -\frac{h}{2}[(\gamma_1-\gamma_3)(\partial_x+\partial_y)-(\gamma_2-\gamma_4)(\partial_x-\partial_y)]r^a+\mathcal{O}(h^2). \tag{34}$$

The hybrid $\mathcal{LP}/\mathcal{FE}$-*Gal* scheme is second-order accurate only for $\gamma_1=\gamma_3$ and $\gamma_2=\gamma_4$, which conditions also make the convective-term discretization dissipation-free, as will be shown in Section 5. Finally, a hybrid *SUPG*/$\mathcal{FE}$-*Gal* scheme can never achieve second-order accuracy, its TE being:

$$\mathrm{TE}^{SUPG/\mathcal{FE}\text{-}Gal} = -\frac{h}{2}(a\partial_x+b\partial_y)r^a+\mathcal{O}(h^2). \tag{35}$$

4. Fourier analysis

This section provides a multidimensional Fourier analysis of the various discretizations considered so far, in order to determine their dissipation and dispersive properties. Such an analysis, together with that of the previous section, will allow one to design a minimum-dispersion-error $\mathcal{RD}$ scheme, which is suitable for the discretization of the convective term in advection–diffusion problems.

Assume that the unknown variable $u(x, y)$ is periodic over the domain $[0, L]^2$, discretized by a uniform Cartesian mesh with $h = L/N$; $u(x, y)$ can be expressed as the summation of Fourier modes:

$$u(x,y)=\sum_{k_x,k_y=-N/2}^{N/2}\hat{u}_{k_x,k_y}\mathrm{e}^{2\pi\mathbb{i}(k_xx+k_yy)/L},$$

where k_x, k_y are the wavenumbers along the x and y directions, respectively, and $\mathbb{i}$ is the imaginary unit. Introducing the dimensionless wavenumbers, β_x, $\beta_y \in [-\pi, \pi]$, and the dimensionless coordinates, s_x and s_y, defined as

$$\begin{cases}\beta_x=\dfrac{2\pi k_x h}{L},\\ \beta_y=\dfrac{2\pi k_y h}{L},\end{cases}\qquad\begin{cases}s_x=\dfrac{x}{h},\\ s_y=\dfrac{y}{h},\end{cases}$$

the Fourier mode can be written as $\mathrm{e}^{\mathbb{i}(s_x\beta_x+s_y\beta_y)}$, which is a planar wave with dimensionless wavevector $\boldsymbol{\beta}=(\beta_x, \beta_y)$, having magnitude $\beta=\sqrt{\beta_x^2+\beta_y^2}$ and direction $\theta=\arctan(\beta_y/\beta_x)$. Then, the semi-discrete form of Eq. (1) at a generic node of the computational domain can be written as

$$\frac{\mathrm{d}u}{\mathrm{d}t}=[\mathcal{R}_h(u)].$$

Therefore, the Fourier analysis of the discrete operator, $\mathcal{R}_h$, provides the following evolution equation for the single mode:

$$\frac{\mathrm{d}u}{\mathrm{d}t}=\mathcal{R}_h^a(u)+\mathcal{R}_h^d(u)=(v\mathcal{Z}^a+\sigma\mathcal{Z}^d)\frac{u}{\Delta t},\quad \mathcal{Z}\in\mathbb{C}, \tag{36}$$

where $v=\|\boldsymbol{\lambda}\|\Delta t/h$ is the Courant number, $\sigma=\mu\Delta t/h^2$, and $\mathcal{Z}^{a-d}=\mathcal{Z}^{a-d}(\beta_x,\beta_y,\delta)$. For a fixed value of the velocity flow angle, δ, the locus of $\mathcal{Z}^{a-d}$ in the complex plane is called *Fourier footprint* and depends *uniquely* on the spatial discretization operator.

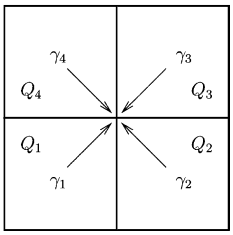

Fig. 5. Cartesian grid.

It is noteworthy that the present approach analyzes, for a given δ, all of the grid-resolved wavenumbers and thus it is not restricted to the case of Fourier modes aligned with the advection velocity (like for example, among others, the analyses of Lele [18], Li [19], and Christon et al. [27,28]).

4.1. Pure advection and the multidimensional modified wavenumber

Consider the case of pure advection, i.e., $\mu = 0$. Indicating with u a solution which has the form of a generic Fourier mode, the gradient of u can be written as

$$\nabla u = \frac{\mathbb{i}}{h}\boldsymbol{\beta} u. \tag{37}$$

The exact derivative of u along the natural coordinate, ξ, is given as

$$\frac{\partial u}{\partial \xi} = \frac{\boldsymbol{\lambda}}{\|\boldsymbol{\lambda}\|}\cdot\nabla u = \frac{\mathbb{i}u}{h}\frac{\boldsymbol{\lambda}}{\|\boldsymbol{\lambda}\|}\cdot\boldsymbol{\beta} = \frac{\mathbb{i}u}{h}\beta\cos(\delta-\theta) = \frac{\mathbb{i}u}{h}\tilde{\beta}, \tag{38}$$

where $\tilde{\beta} = \beta\cos(\delta-\theta)$ can be considered as the generalization of the wavenumber for two-dimensional convection. The approach usually employed for the dispersion analysis in two dimensions is based on the concept of numerical anisotropy [17–19] and implies that the Fourier mode is aligned with the advection velocity. Here, a more general multidimensional analysis is performed, which treats the advection angle, δ, and the Fourier mode angle, θ, as independent parameters. Therefore, it is possible to evaluate the amplitude and dispersion errors of all Fourier modes ($-\pi \leqslant \theta \leqslant \pi$), for any advection angle. The *modified wavevector*, $\boldsymbol{\beta}'$, corresponding to a discrete approximation, $(\nabla u)_{\mathrm{num}}$, of the gradient of u is defined as

$$(\nabla u)_{\mathrm{num}} = \frac{\mathbb{i}}{h}\boldsymbol{\beta}' u, \tag{39}$$

and the numerical derivative of u along ξ is

$$\left(\frac{\partial u}{\partial \xi}\right)_{\mathrm{num}} = \frac{\boldsymbol{\lambda}}{\|\boldsymbol{\lambda}\|}\cdot(\nabla u)_{\mathrm{num}} = \frac{\mathbb{i}u}{h}(\beta'_x\cos(\delta)+\beta'_y\sin(\delta)) = \frac{\mathbb{i}u}{h}\tilde{\beta}', \tag{40}$$

where $\tilde{\beta}'$ is the two-dimensional generalization of the modified wavenumber.

Considering that

$$\|\boldsymbol{\lambda}\|\left(\frac{\partial u}{\partial \xi}\right)_{\mathrm{num}} = -\frac{\mathrm{d}u}{\mathrm{d}t} = -\frac{v\mathcal{Z}^a}{\Delta t}u, \tag{41}$$

and employing Eq. (40), one has

$$\tilde{\beta}' = \mathbb{i}\mathcal{Z}^a. \tag{42}$$

Assuming an exact integration in time, the amplification factor is

$$G = \mathrm{e}^{v\mathcal{Z}^a}; \tag{43}$$

thus, $\mathrm{Re}(\mathcal{Z}^a) = \mathrm{Im}(\tilde{\beta}')$ and $\mathrm{Im}(\mathcal{Z}^a) = -\mathrm{Re}(\tilde{\beta}')$ provide the dissipation and dispersion properties of the scheme, respectively. It is well known that centred schemes are characterized by a pure imaginary $\mathcal{Z}^a$, thereby adding no spurious dissipation to the convective term, in contrast to upwind schemes, having a non-zero real part of $\mathcal{Z}^a$. It is also worth remarking that the modified wavenumber $\tilde{\beta}'$ allows one to compare the multidimensional spectral properties of different schemes, such as $\mathcal{FD}$, $\mathcal{FE}$ and compact (Padé-type) schemes. For example, the modified wavenumber of a compact scheme can be computed as

$$\tilde{\beta}' = \cos(\delta)\beta'_x(\beta_x) + \sin(\delta)\beta'_y(\beta_y),$$

where β'_x and β'_y depend on the discretization of the derivatives of u with respect to x and y, respectively, and are given in several well-known publications for many schemes of interest, see, e.g., [18].

Appendix B provides the analytical expressions of the real part of $\mathcal{Z}^a$ and of the real part of the modified wavenumber $\tilde{\beta}'$, which are used in the following to characterize the dissipative and dispersive properties of the considered schemes.

In order to analyze the properties of $\mathcal{RD}$ schemes, their amplification factors have been computed and the contour lines of the corresponding magnitudes, $|G|$, are shown in Figs. 6–8 for different advection angles, δ, and $v = 1$. Obviously, for the considered case of pure advection, $|G|_{\mathrm{ex}} = 1$. The figures indicate that multidimensional $\mathcal{LP}$ schemes are characterized by a contour pattern with $|G|$ close to one in an elongated region perpendicular to the advection velocity. This means that the Fourier modes oscillating in the direction normal to $\boldsymbol{\lambda}$ are barely damped. This is due to the multidimensional nature of such schemes, in contrast to the behav-

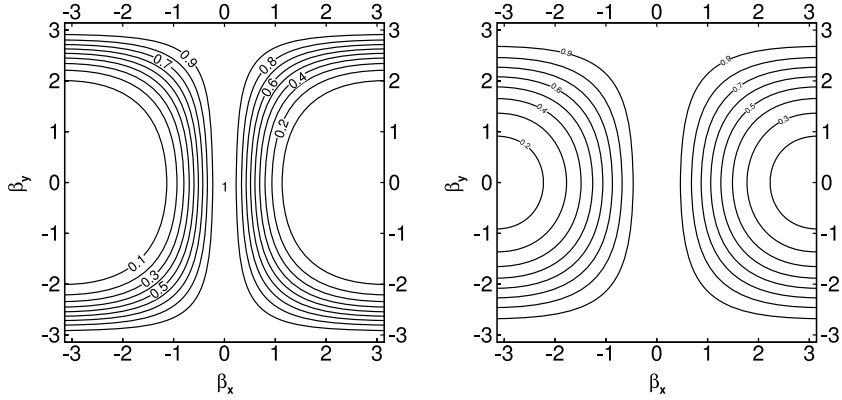

Fig. 6. Amplification factor for the *LDA* (left) and *LW* (right) schemes for $\delta = 0$.

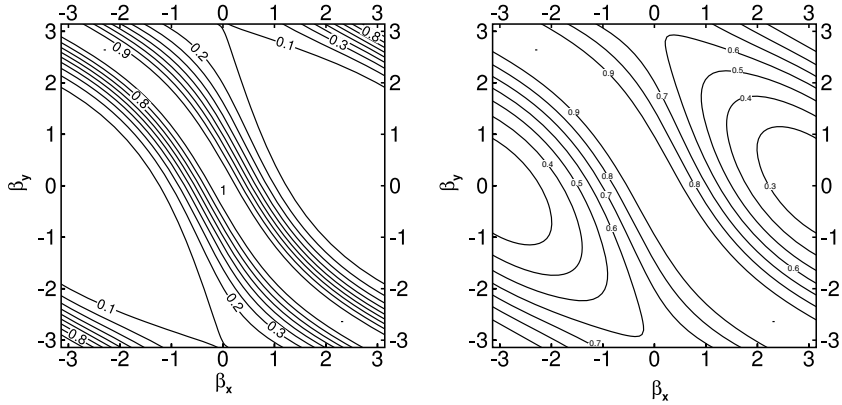

Fig. 7. Amplification factor for the *LDA* (left) and *LW* (right) schemes for $\delta = \pi/6$.

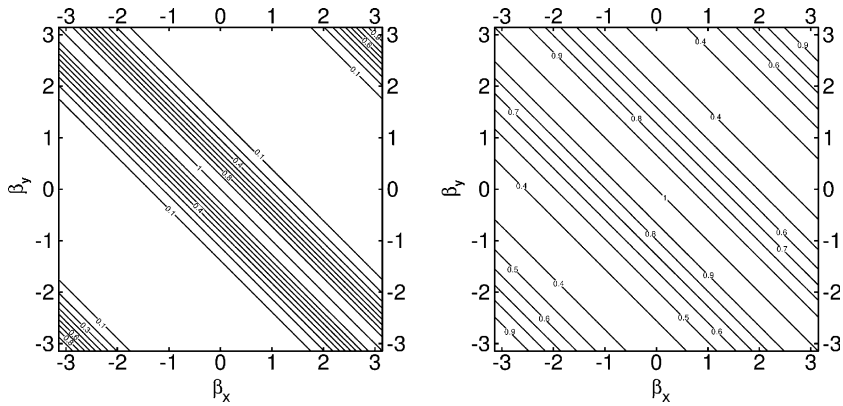

Fig. 8. Amplification factor for the *LDA* (left) and *LW* (right) schemes for $\delta = \pi/4$.

ior shown by classical dimensionally-split upwind schemes, see Fig. 9, which provides an isotropic contour pattern for $|G|$ except for the case $\delta = 0$. In this case in fact, the one-dimensional configuration is recovered and the spectral properties (dissipation and dispersion) are independent of β_y. Comparing the *LDA* and *LW* schemes for quadrilaterals (Figs. 6–8), the latter scheme appears to be less dissipative. Furthermore, unlike their triangle-based counterparts, which are shown in Fig. 10, for $\delta = \pi/6$, the values of $|G|$ are equal to one for $(\beta_x, \beta_y) = (\pm\pi, \pm\pi)$. This is due to the fact that the values of $\mathcal{Z}^a$ for high frequency modes cluster near the origin of the complex plane, since

$$\lim_{\beta_x,\beta_y\to\pm\pi} \mathcal{Z}^a(\beta_x, \beta_y, \delta) = \mathcal{Z}^a(\beta_x = \pm\pi, \beta_y = \pm\pi, \delta) = 0, \tag{44}$$

which is valid for all $\mathcal{LP}$ schemes on quadrilaterals. Therefore, for $Q1$ elements, the following proposition holds.

Proposition 2. *If a linear scheme is $\mathcal{LP}$, then its Fourier footprint $\mathcal{Z}^a$ is constrained by Eq. (44).*

Proof. Consider a generic node i and the computational cells $\Omega_E \in \Delta_i$. For each Ω_E, the *elemental Fourier footprint*, $\mathcal{Z}^{E,a}$, with respect to node i, can be obtained as follows. Express the fluctuation, $\phi^{E,a}$, as a function of the solution at the vertices of the element. For example, referring to Fig. 3, the fluctuation on the lower left element $Q1$ is computed as

$$\frac{h}{2}\|\boldsymbol{\lambda}\|[(u_i - u_j + u_k - u_q)\cos(\delta) + (u_i - u_j - u_k + u_q)\sin(\delta)]. \tag{45}$$

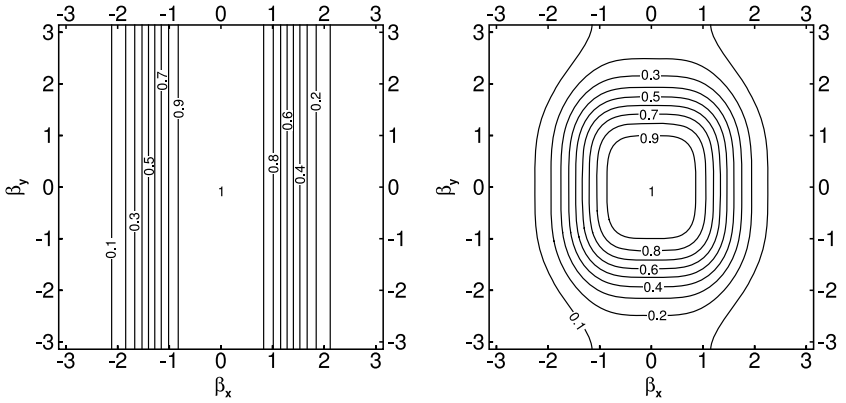

Fig. 9. Amplification factor for the second-order accurate (fully) upwind $\mathcal{FD}$ scheme with $\delta = 0$ (left) and $\delta = \pi/6$ (right).

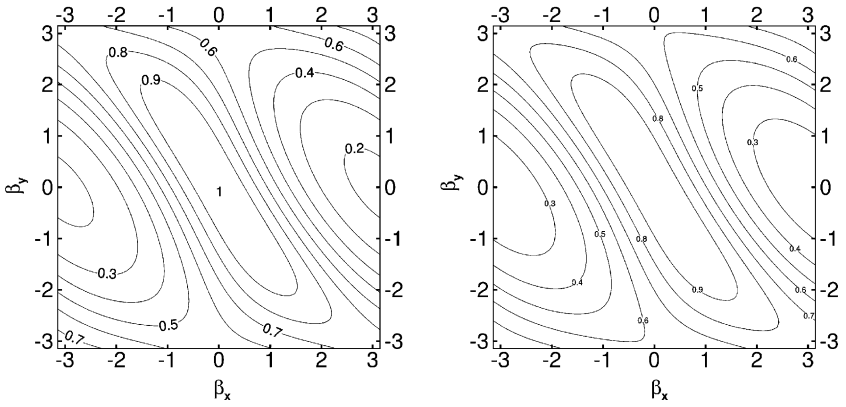

Fig. 10. Amplification factor for the *LDA* (left) and *LW* (right) schemes on a uniform triangulation and $\delta = \pi/6$.

Then, substitute the Fourier mode into the general expression above, to get

$$\phi^{E,a} = -|\Omega_i| \frac{v\mathcal{Z}^{E,a}}{\Delta t} u_i. \tag{46}$$

Using this procedure, one obtains the following expressions of the Fourier footprint for each element sharing node i (see Fig. 3):

$$\begin{aligned}
\mathcal{Z}^{Q_1,a} &= -2\mathrm{i}\mathrm{e}^{-\frac{\mathrm{i}}{2}(\beta_x+\beta_y)}A,\\
\mathcal{Z}^{Q_2,a} &= -2\mathrm{i}\mathrm{e}^{\frac{\mathrm{i}}{2}(\beta_x-\beta_y)}A,\\
\mathcal{Z}^{Q_3,a} &= -2\mathrm{i}\mathrm{e}^{\frac{\mathrm{i}}{2}(\beta_x+\beta_y)}A,\\
\mathcal{Z}^{Q_4,a} &= -2\mathrm{i}\mathrm{e}^{-\frac{\mathrm{i}}{2}(\beta_x-\beta_y)}A,
\end{aligned} \tag{47}$$

where

$$A = \sin\left(\frac{\beta_x}{2}\right)\cos\left(\frac{\beta_y}{2}\right)\cos(\delta) + \cos\left(\frac{\beta_x}{2}\right)\sin\left(\frac{\beta_y}{2}\right)\sin(\delta).$$

Considering that

$$|\Omega_i|\frac{\mathrm{d}u_i}{\mathrm{d}t} = -\sum_{\Omega_E\in\Delta_i}\phi_i^{E,a} = -\sum_{\Omega_E\in\Delta_i}\gamma_i^E\phi^{E,a},$$

and using Eqs. (36) and (46), one has

$$\mathcal{Z}^a = \sum_{\Omega_E\in\Delta_i}\gamma_i^E\mathcal{Z}^{E,a}. \tag{48}$$

From Eq. (47) it appears that condition (44) holds for any $\mathcal{Z}^{E,a}$, and thus also for $\mathcal{Z}^a$, provided that the distribution coefficients γ_i^E are bounded. □

As a consequence, the amplification factor for high frequencies is very close to one (reaching one for the highest resolved wavenumbers), whatever time discretization is employed and regardless of the chosen Courant number, v. As an example, if the derivative in the ODE (36) is discretized by an n-stage Runge–Kutta scheme with coefficients $c_1, c_2, \ldots, c_{n-1}, c_n$, the resulting amplification factor reads

$$G(\mathcal{Z}) = 1 + c_n v\mathcal{Z}(1 + c_{n-1}v\mathcal{Z}(\cdots(1 + c_1 v\mathcal{Z}))). \tag{49}$$

Eq. (49) defines the stability domain of the Runge–Kutta time operator in the complex plane. It is immediate to verify that the amplification factor at the origin of the complex plane is equal to one. Another way to explain the phenomenon described above is the following: if we consider a checkerboard (maximum frequency) mode, the fluctuation on each element is zero, so the signals for an $\mathcal{LP}$ scheme will be zero as well. As a consequence, the mode will not be dissipated nor propagated. This behavior is very similar to that observed when using centred $\mathcal{FD}$ schemes. It is noteworthy that numerical experiments prove that the high frequency modes have low or no damping even on non Cartesian grids. Finally, the Fourier footprint of the *SUPG* method, which is not $\mathcal{LP}$, is not constrained by Eq. (44), and, as shown in Fig. 11, the magnitude of its amplification factor is less than one for $(\beta_x, \beta_y) = (\pm\pi, \pm\pi)$. In conclusion, the analysis above indicates that $\mathcal{LP}$ schemes, when applied to quadrilateral cells, are marginally stable for any value of the Courant number, so that they require additional dissipation to compute pure advection problems. Indeed, $\mathcal{LP}$ schemes can be effectively stabilized by an artificial-dissipation (AD) term without affecting their order of accuracy. A simple strategy is proposed here, namely, adding the bias term of the *SUPG* scheme to the signals of the original $\mathcal{LP}$ scheme:

$$\phi_i^{E,a} = \gamma_i^{\mathcal{LP}}\phi^{E,a} + \phi_i^{\mathrm{bias}}, \quad \phi_i^{\mathrm{bias}} = \int_{\Omega_E}\tau(\boldsymbol{\lambda}\cdot\boldsymbol{\nabla}N_i)\boldsymbol{\nabla}\cdot\mathbf{f}_h\,\mathrm{d}\Omega. \tag{50}$$

Notice that such a scheme has the same dispersion error as the original $\mathcal{LP}$ one, but a greater dissipation error, due to the added AD. For example, the amplification factor of the *LDA* scheme with AD is shown in Fig. 12.

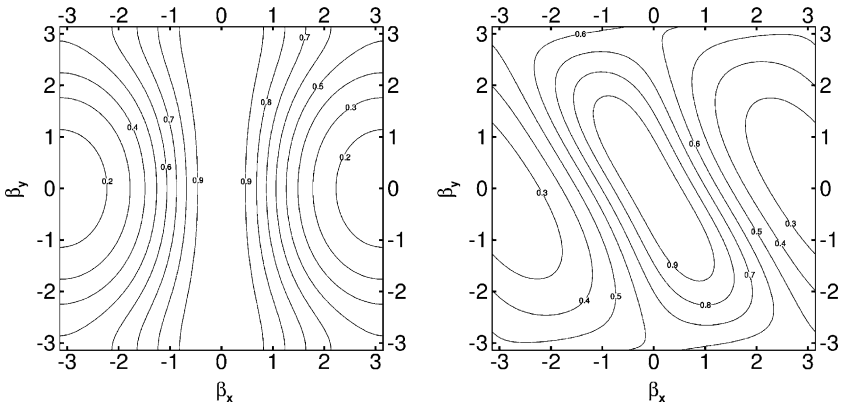

Fig. 11. Amplification factor for the *SUPG* scheme with $\delta = 0$ (left) and $\delta = \pi/6$ (right).

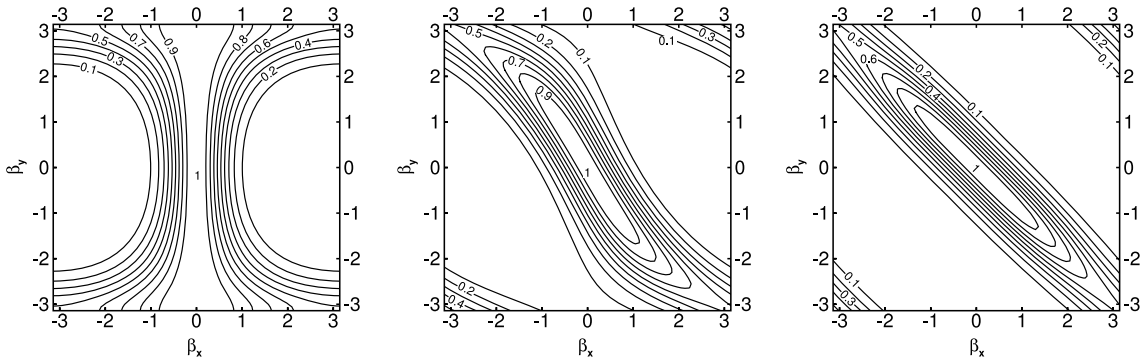

Fig. 12. *LDA* scheme with AD: amplification factor error for the advection equation with $\delta = 0$ (left), $\delta = \pi/6$ (center) and $\delta = \pi/4$ (right).

The dispersive properties of $\mathcal{RD}$ schemes are presented in terms of the dispersion error, $\mathrm{Re}(\tilde{\beta}') - \tilde{\beta}$. Figs. 13–15 provide the contour lines in the (β_x, β_y) plane, for different advection angles, δ. The *LDA* and *LW* schemes provide very similar contour patterns, which are also very close to those obtained on triangular cells, which are given in Fig. 16 for the case $\delta = \pi/6$. The dispersion error obtained using the second-order accurate centred and (fully) upwind $\mathcal{FD}$ schemes, the fourth-order accurate scheme of [24], the standard fourth-order accurate $\mathcal{FD}$ scheme, which requires a wider stencil, and the Padé scheme are also reported in Figs. 18–21, for comparison.

It has already been mentioned that the bias term of the artificial dissipation used to stabilize $\mathcal{LP}$ schemes is purely dissipative and does not alter the dispersive properties of the underlying $\mathcal{LP}$ scheme. Therefore, the *SUPG* scheme has the same dispersion error as that of the $\mathcal{FE}$-*Gal* one and thus of the scheme of Abarbanel and Kumar [24]. Moreover, some other well-known schemes share the same dispersive characteristics. Indeed, the following relations will be derived:

$$\mathrm{Re}(\tilde{\beta}'^{\mathcal{FD}-\mathrm{upw1}}) = \mathrm{Re}(\tilde{\beta}'^{\mathcal{FD}\text{-}\mathrm{cen2}}), \tag{51}$$

$$\mathrm{Re}(\tilde{\beta}'^{LDA}) = \mathrm{Re}(\tilde{\beta}'^{N}), \tag{52}$$

$$\mathrm{Re}(\tilde{\beta}'^{LW}) = \mathrm{Re}(\tilde{\beta}'^{\mathcal{RD}\text{-}\mathrm{cen}}), \tag{53}$$

where $\mathcal{FD}$-upw1 stands for the $\mathcal{FD}$ first-order upwind scheme, $\mathcal{FD}$-cen2 stands for the $\mathcal{FD}$ second-order centred scheme, and $\mathcal{RD}$-cen stands for the $\mathcal{RD}$ centred scheme (fluctuation equally distributed among the nodes).

Eq. (51) stems from a multidimensional generalization of the results achieved by Li [19]. In particular, considering a computational stencil with $2N + 1$ points in one dimension, the centred scheme is characterized by a formal accuracy of order $2N$, while the most accurate upwind-biased scheme reaches an accuracy

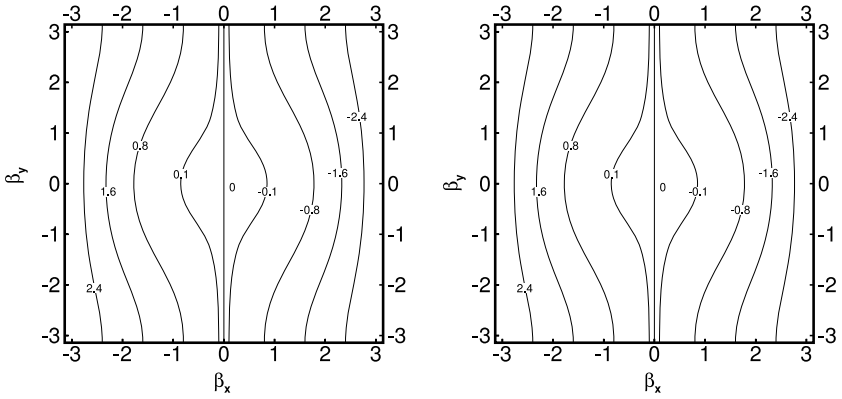

Fig. 13. Dispersion error for the *LDA* (left) and *LW* (right) schemes for $\delta = 0$.

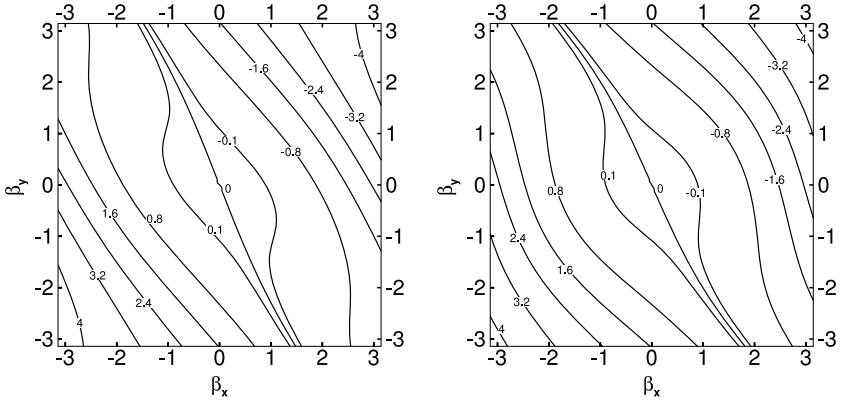

Fig. 14. Dispersion error for the *LDA* (left) and *LW* (right) schemes for $\delta = \pi/6$.

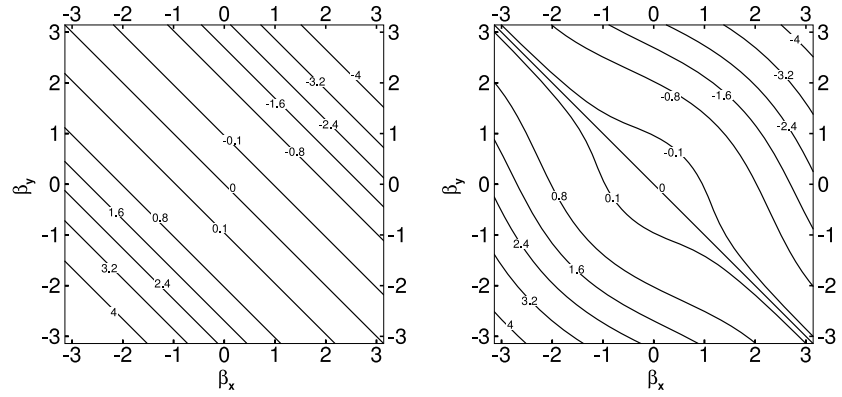

Fig. 15. Dispersion error for the *LDA* (left) and *LW* (right) schemes for $\delta = \pi/4$.

of order $2N - 1$. It is shown in [19] that the centred and upwind-biased schemes have the same dispersion characteristics, their only difference consisting in the dissipation of the upwind-biased scheme. In a similar way, one sees that *LDA* and *N* schemes have the same dispersion error and differ only for the dissipation one, see Eq. (52), which is obtained directly by the Fourier footprints of the two schemes reported in Appendix B.

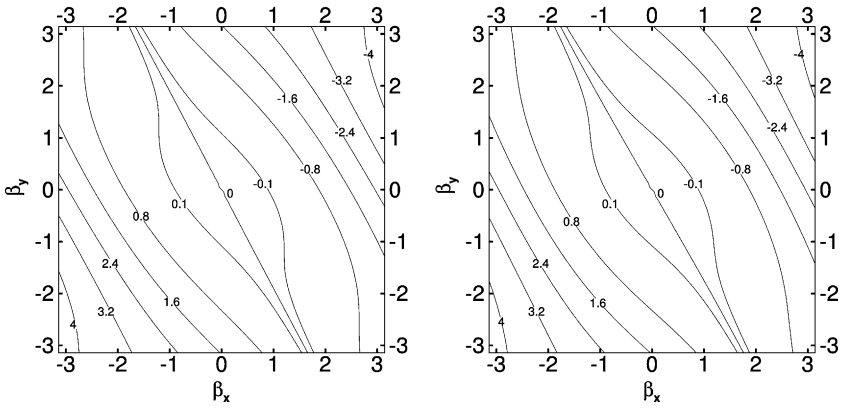

Fig. 16. Dispersion error for the *LDA* (left) and *LW* (right) schemes on a uniform triangulation and $\delta = \pi/6$.

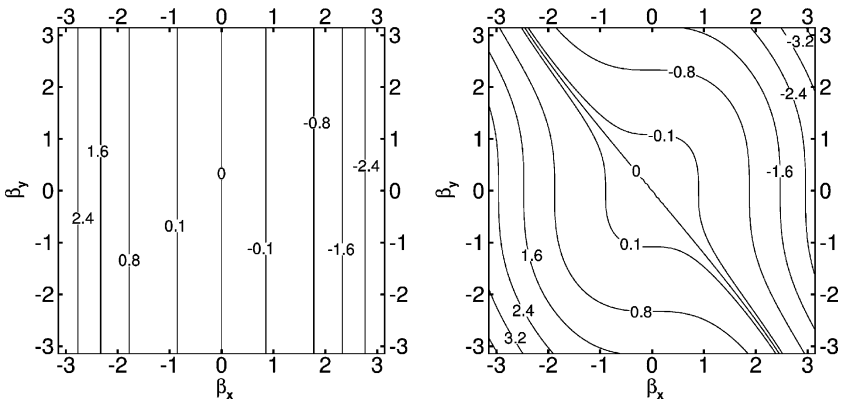

Fig. 17. Dispersion error for the second-order accurate centred $\mathcal{FD}$ scheme with $\delta = 0$ (left) and $\delta = \pi/6$ (right).

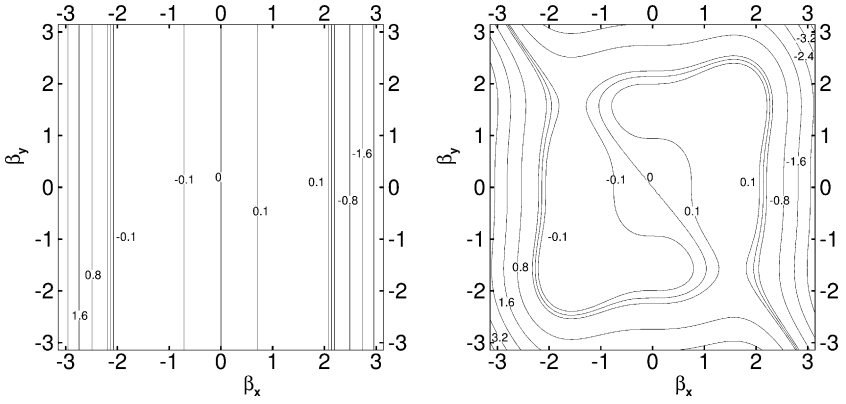

Fig. 18. Dispersion error for the second-order accurate (fully) upwind $\mathcal{FD}$ scheme with $\delta = 0$ (left) and $\delta = \pi/6$ (right).

Finally, the *LW* scheme relies on the upwind parameters k_j which are based on the normal to the diagonals. With reference to Fig. 5, since $\mathbf{n}_1 = -\mathbf{n}_3$ and $\mathbf{n}_2 = -\mathbf{n}_4$, it follows that $k_1 = -k_3$ and $k_2 = -k_4$. As a consequence, the *LW* distribution coefficients can be written as

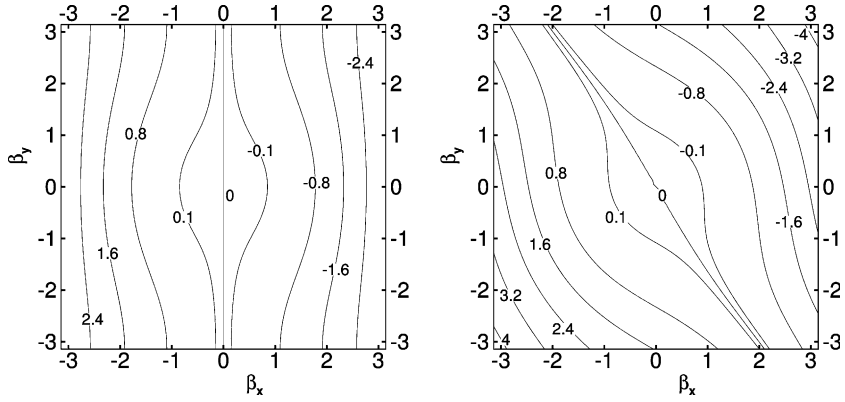

Fig. 19. Dispersion error for the fourth-order accurate scheme of [24] with $\delta = 0$ (left) and $\delta = \pi/6$ (right).

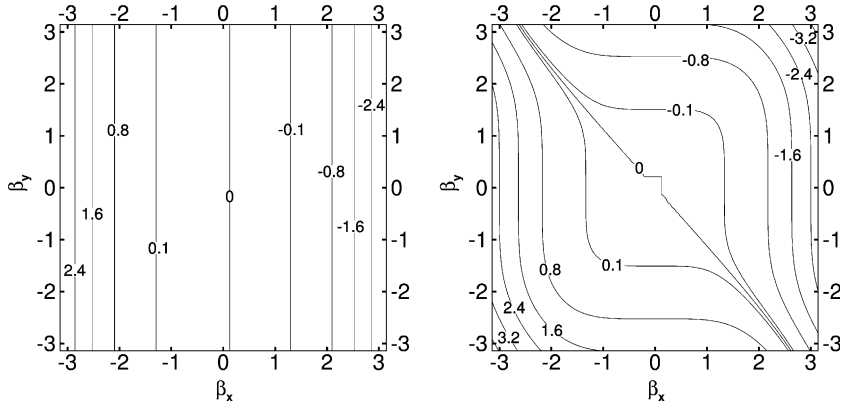

Fig. 20. Dispersion error for the fourth-order accurate centred $\mathcal{FD}$ scheme with $\delta = 0$ (left) and $\delta = \pi/6$ (right).

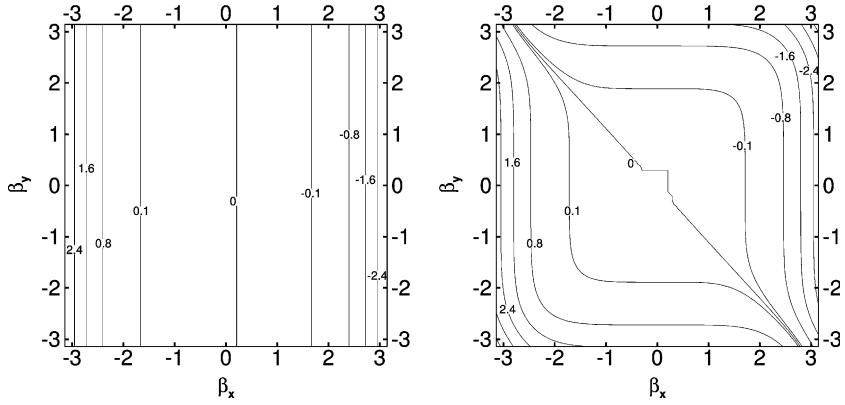

Fig. 21. Dispersion error for the fourth-order accurate centred compact scheme with $\delta = 0$ (left) and $\delta = \pi/6$ (right).

$$\gamma_1 = \frac{1}{4} + \epsilon, \quad \gamma_2 = \frac{1}{4} + \varsigma, \quad \gamma_3 = \frac{1}{4} - \epsilon, \quad \gamma_4 = \frac{1}{4} - \varsigma, \tag{54}$$

where ϵ and ς are functions of the parameters k_j. Furthermore, according to Eq. (47), the imaginary parts of the Fourier footprints relative to opposite elements are equal, namely:

$$\begin{aligned} \mathrm{Im}(\mathcal{Z}^{Q_1,a}) &= \mathrm{Im}(\mathcal{Z}^{Q_3,a}), \\ \mathrm{Im}(\mathcal{Z}^{Q_2,a}) &= \mathrm{Im}(\mathcal{Z}^{Q_4,a}). \end{aligned} \tag{55}$$

Therefore, since the elemental Fourier footprints are combined according to Eq. (48), with the coefficients given by Eq. (54), non-centred contributions relative to opposite elements cancel out, leading to Eq. (53); it is noteworthy that the same relationship can be obtained, using a similar procedure, also for a uniform triangulation.

A few final considerations about the spectral properties of the considered schemes are in order. The dispersion error provided by the second-order accurate (fully) upwind scheme is slightly smaller than that of the centred one, which is very close to the errors of $\mathcal{RD}$ schemes and of the fourth-order accurate one of [24]. Moreover, unlike the dissipation error, the dispersion error of *explicit* (non compact) schemes is mostly dependent on the extent of the computational molecule. In fact, the dispersion error of the fourth-order accurate $\mathcal{FD}$ centred scheme, shown in Fig. 20, is lower than the one produced by the scheme of [24], due to its larger stencil. This is not true when using a compact scheme; in fact, the dispersion error provided by $\mathcal{RD}$ schemes appears markedly larger than that given by the centred Padé one using the same stencil (see Fig. 21).

4.2. Pure diffusion equation

Consider now the case of pure diffusion ($\nabla \cdot \mathbf{f} = 0$ in Eq. (1)). For a solution u which has the form of a generic Fourier mode, the Laplacian of u can be written as

$$\nabla^2 u = -\frac{\beta^2}{h^2} u. \tag{56}$$

On the other hand, its discrete approximation $(\nabla^2 u)_{\mathrm{num}}$ can be expressed as

$$(\nabla^2 u)_{\mathrm{num}} = -\frac{\beta''}{h^2} u, \tag{57}$$

where, in general, $\beta'' \in \mathbb{C}$. Considering that

$$(\nabla^2 u)_{\mathrm{num}} = \frac{\mathrm{d}u}{\mathrm{d}t} = \frac{\sigma \mathcal{Z}^d}{\Delta t} u, \tag{58}$$

and employing Eq. (57), one has

$$\beta'' = -\mathcal{Z}^d. \tag{59}$$

Again, it can be noticed that the introduction of the function β'' allows one to analyze and compare *explicit* and compact schemes for the discretization of the diffusion term within a single mathematical framework. Assuming an exact time integration, the amplification factor is given as

$$G = \mathrm{e}^{\sigma \mathcal{Z}^d}.$$

As a result, the dissipative and dispersive properties of the scheme are given by $\mathrm{Re}(\mathcal{Z}^d) = -\mathrm{Re}(\beta'')$ and $\mathrm{Im}(\mathcal{Z}^d) = -\mathrm{Im}(\beta'')$, respectively. Centred schemes, being characterized by a real function β'', are purely dissipative. A non-centred approach introduces instead some dispersion. Obviously, in the case of pure diffusion, a centred approach is the only suitable choice, but this may not be the case for advection–diffusion problems, as shown in the following section. In the present analysis, two schemes have been considered for the pure diffusion equation, namely, the centred $\mathcal{RD}$ and $\mathcal{FE}$-*Gal* schemes, their Fourier footprints being provided in Appendix C, for completeness. Here, the contour lines of the amplification factor error, $|G| - |G|_{\mathrm{ex}}$, where $G_{\mathrm{ex}} = \exp(-\sigma\beta^2)$, in the (β_x, β_y) plane, for the case $\sigma = 1$, are given in Figs. 22 and 23 for a uniform Cartesian grid and a uniform triangulation, respectively. Fig. 22 shows that the $\mathcal{FE}$ Galerkin scheme is able to damp all frequencies. On the other hand, a residual based approach leads to values of $|G|$ equal to one for $\beta_x = \pm\pi$ or $\beta_y = \pm\pi$. This means that the Fourier modes with the highest frequency are not damped, violating the dissipative nature of the term, because the values of $\mathcal{Z}^d$ for high frequency modes cluster near the origin of the complex plane, namely

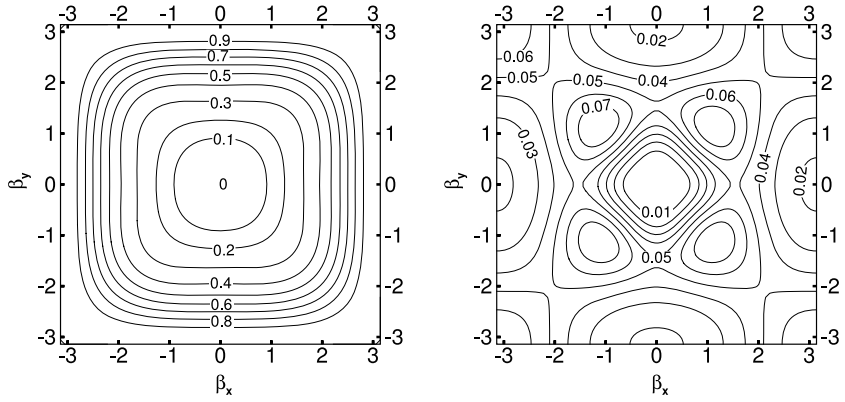

Fig. 22. Amplification factor error for the centred $\mathcal{RD}$ scheme (left) and $\mathcal{FE}$ Galerkin scheme (right) for quadrilateral cells.

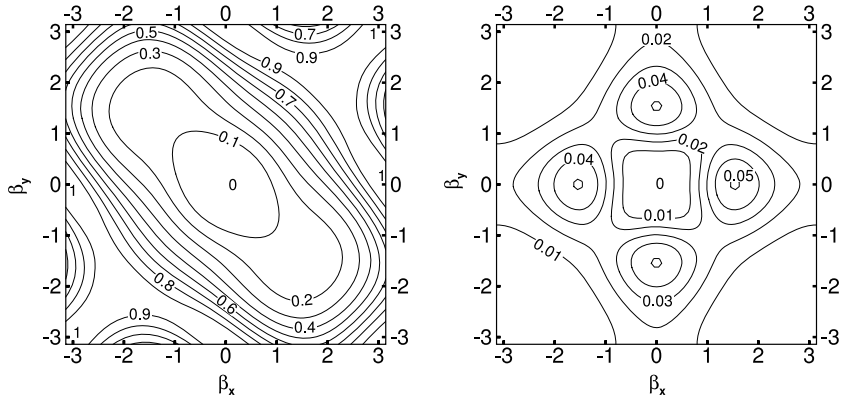

Fig. 23. Amplification factor error for the centred $\mathcal{RD}$ scheme (left) and the $\mathcal{FE}$ Galerkin scheme (right) on a uniform triangulation.

$$\lim_{\beta_x \to \pm\pi} \mathcal{Z}^d(\beta_x, \beta_y) = \mathcal{Z}^d(\beta_x = \pm\pi, \beta_y) = 0, \tag{60}$$

$$\lim_{\beta_y \to \pm\pi} \mathcal{Z}^d(\beta_x, \beta_y) = \mathcal{Z}^d(\beta_x, \beta_y = \pm\pi) = 0, \tag{61}$$

which are valid for all $\mathcal{LP}$ residual distribution schemes.

Proposition 3. *If a linear scheme for the discretization of the diffusion term on quadrilateral elements is $\mathcal{LP}$, then its Fourier footprint $\mathcal{Z}^d$ is constrained by Eqs. (60) and (61).*

Proof. Consider a generic node i and the computational cells $\Omega_E \in \Delta_i$. For each Ω_E, the *elemental Fourier footprint*, $\mathcal{Z}^{E,d}$, with respect to node i, can be obtained as follows. Express the fluctuation, $\phi^{E,d}$, as a function of the solution at the vertices of the element. For example, referring to the notation of Fig. A.1, the diffusive fluctuation on the lower left element $Q1$ of Fig. 3 is computed as

$$-\frac{\mu}{4}(-u_e - u_f - u_h + 2u_i - u_j - u_k - u_m - u_n + 2u_o + 2u_p + 2u_q - u_w). \tag{62}$$

Then, substitute the Fourier mode into the general expression above to get

$$\phi^{E,d} = |\Omega_i| \frac{\sigma \mathcal{Z}^{E,d}}{\Delta t} u_i. \tag{63}$$

Using this procedure, the following expressions for the Fourier footprint are obtained for each element sharing node i (see Fig. 3):

the convective fluctuation and the $\mathcal{FE}$ Galerkin scheme for discretizing the diffusion term, leads to a first-order accurate scheme. On the other hand, it was shown that distributing the whole fluctuation (convective plus diffusive) by an $\mathcal{LP}$ scheme provides second-order accuracy. Fig. 24 show the amplification factor errors, $|G| - |G|_{\mathrm{ex}}$, in the (β_x, β_y) plane, of the *LDA–LDA* scheme, for values of the (numerical) Peclet number, $Pe = v/\sigma$, equal to 0.1 and 1.5, respectively. For the lower value of Pe, the error is greater than one at the upper-right and lower-left corners of the plane, indicating that some high frequency modes are amplified. Indeed, $\mathcal{RD}$ schemes are unsuitable to discretize the diffusion term insofar as they introduce undamped high-frequency modes. In the case of advection–diffusion problems, this amplification can be effectively balanced by the dissipative effect due to the upwind treatment of the convective term, provided that Pe is sufficiently high. Nishikawa and Roe [26] proposed to employ an upwind scheme continuously switching towards a centred discretization as Pe decreases, in order to treat advection–diffusion problems for any value of Pe. However, such a strategy, being based on an $\mathcal{RD}$ approach, shows poor stability properties for diffusion dominated problems.

5. Minimum dispersion error $\mathcal{RD}$ scheme

The truncation error and Fourier analyses provided so far are used in this section to design a second-order accurate minimum-dispersion error $\mathcal{RD}$ $\mathcal{LP}$ scheme which is suitable for the discretization of the convective term in advection–diffusion problems. A generic $\mathcal{LP}$ scheme on quadrilateral elements is characterized by four degrees of freedom, see Fig. 25. From Eq. (34) it appears that a hybrid $\mathcal{LP}/\mathcal{FE}$-*Gal* scheme with $\gamma_1 = \gamma_3$ and $\gamma_2 = \gamma_4$ provides second-order accuracy for the advection–diffusion equation. It is noteworthy that a distribution scheme for the pure advection equation which satisfies the two conditions above does not introduce any spurious dissipation, namely, it is purely dispersive. This property can be demonstrated looking at the Fourier footprint of the elements contributing to each node in the case of pure advection, given by Eq. (47). In fact, the real parts of the Fourier footprints of the four elements read:

$$\begin{aligned} \mathrm{Re}(\mathcal{Z}^{Q_1,a}) &= -\mathrm{Re}(\mathcal{Z}^{Q_3,a}) = \frac{1}{2}[\mathfrak{R}_{1x}\cos(\delta) + \mathfrak{R}_{1y}\sin(\delta)], \\ \mathrm{Re}(\mathcal{Z}^{Q_2,a}) &= -\mathrm{Re}(\mathcal{Z}^{Q_4,a}) = \frac{1}{2}[\mathfrak{R}_{2x}\cos(\delta) + \mathfrak{R}_{2y}\sin(\delta)], \end{aligned} \tag{69}$$

where

$$\begin{aligned} \mathfrak{R}_{1x} &= -1 + \cos(\beta_x) - \cos(\beta_y) + \cos(\beta_x + \beta_y), \\ \mathfrak{R}_{1y} &= -1 - \cos(\beta_x) + \cos(\beta_y) + \cos(\beta_x + \beta_y), \\ \mathfrak{R}_{2x} &= 1 - \cos(\beta_x) + \cos(\beta_y) - \cos(\beta_x - \beta_y), \\ \mathfrak{R}_{2y} &= -1 - \cos(\beta_x) + \cos(\beta_y) + \cos(\beta_x - \beta_y). \end{aligned}$$

Since opposite elements have opposite Fourier-footprint real parts, conditions

$$\gamma_1 = \gamma_3 \quad \text{and} \quad \gamma_2 = \gamma_4 \tag{70}$$

guarantee zero dissipation at each node. Thus, considering that the distribution coefficients must sum up to one, for conservation, a one-parameter class of zero dissipation schemes exists. Needless to say, the centred scheme, with $\gamma_1 = \gamma_2 = \gamma_3 = \gamma_4 = 1/4$, belongs to this class.

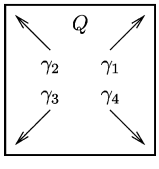

Fig. 25. Degrees of freedom for an $\mathcal{LP}$ scheme.

The modified wavenumber for this one-parameter class of schemes reads

$$\tilde{\beta}' = 2\left[\cos\left(\frac{\beta_y}{2}\right)\cos(\delta)\sin\left(\frac{\beta_x}{2}\right) + \cos\left(\frac{\beta_x}{2}\right)\sin\left(\frac{\beta_y}{2}\right)\sin(\delta)\right] \cdot \left[\cos\left(\frac{\beta_x - \beta_y}{2}\right) - 4\sin\left(\frac{\beta_x}{2}\right)\sin\left(\frac{\beta_y}{2}\right)\gamma_1\right]. \tag{71}$$

Starting from this formula, an optimal dispersion scheme can be designed by minimizing the L_2 norm of the dispersion error, $\mathrm{Re}(\tilde{\beta}') - \tilde{\beta}$, over a portion $[-\varpi, \varpi]^2$ of the frequency domain, namely,

$$L_2 = \frac{1}{4\varpi^2}\left(\int_{-\varpi}^{\varpi}\int_{-\varpi}^{\varpi}[\mathrm{Re}(\tilde{\beta}') - \tilde{\beta}]^2 \mathrm{d}\beta_x \mathrm{d}\beta_y\right)^{1/2}. \tag{72}$$

This procedure leads to the following distribution coefficients:

$$\begin{aligned} \gamma_1^{\mathrm{O}} &= \gamma_3^{\mathrm{O}} = \frac{1}{4} - \psi\sin(2\delta), \\ \gamma_2^{\mathrm{O}} &= \gamma_4^{\mathrm{O}} = \frac{1}{4} + \psi\sin(2\delta), \end{aligned} \tag{73}$$

where $\psi \in \mathbb{R}^+$. If one applies the minimization process over the entire frequency domain, $\varpi = \pi$, the coefficient ψ is equal to 7/12 and the scheme is referred here as the Opt scheme. Notice that some authors, see, e.g., [19], perform the optimization considering only the low-frequency portion of the Fourier spectrum, since $\mathcal{RD}$ schemes are characterized by high dispersion errors for the highest wavenumbers anyway. Following this strategy, namely, choosing $\varpi = \pi/2$, the value of ψ which minimizes L_2 is $\psi = 0.425$.

When the flow is aligned with the mesh ($\delta = 0$), the Opt scheme coincides with the centred one, whose dispersion error is equal to that of the LW scheme, shown in Fig. 13 (right), because of Eq. (53). For $\delta \neq 0$, the Opt scheme provides a smaller dispersion error with respect to either any other $\mathcal{LP}$ scheme or the centred $\mathcal{FD}$ one, see Figs. 14, 17, and 19; furthermore, as shown in Fig. 26 for the case $\delta = \pi/6$, the dispersion error of the optimal scheme is closer to that provided by the fourth-order accurate centred $\mathcal{FD}$ scheme, see Fig. 21. Therefore, this scheme can indeed be considered optimal for discretizing the advection operator within the class of *explicit* schemes with a nine-point stencil. It is noteworthy that the optimization procedure proposed here aims at providing a suitable discretization scheme of the advection operator in advection–diffusion problems, since the minimization of the error is performed on the complete frequency plane. For pure advection problems, it would be suitable to minimize the errors in the direction perpendicular to the advection velocity, the projection of the solution gradient onto the advection direction being zero. Furthermore, the Opt scheme, being characterized by zero dissipation, needs an AD mechanism to be employed for advection dominated problems. Here, the same strategy described previously for $\mathcal{LP}$ schemes, see Eq. (50), is employed, namely, adding a dissipative bias which does not alter the dispersion properties of the scheme:

$$\phi_i^{E,a} = \gamma_i^O \phi^{E,a} + \phi_i^{\mathrm{bias}}. \tag{74}$$

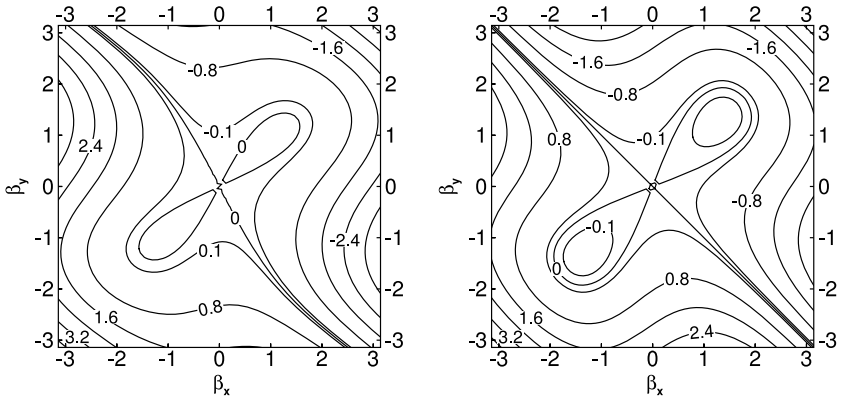

Fig. 26. Optimal scheme: dispersion error for the advection equation with $\delta = \pi/6$ (left) and $\delta = \pi/4$ (right).

Since the Opt scheme is not dissipative, the amplification factor error of the Opt-AD scheme of Eq. (74) coincides with that of the *SUPG* scheme shown in Fig. 11.

Consider now the case of *pure diffusion*. It can be shown in a similar way that the Fourier footprints relative to opposite elements ($Q_1 - Q_3$ and $Q_2 - Q_4$) are symmetrical with respect to the real axis of the complex plane, namely,

$$\begin{cases} \mathrm{Re}(\mathcal{Z}^{Q_1,d}) = \mathrm{Re}(\mathcal{Z}^{Q_3,d}), \\ \mathrm{Re}(\mathcal{Z}^{Q_2,d}) = \mathrm{Re}(\mathcal{Z}^{Q_4,d}), \end{cases} \quad \begin{cases} \mathrm{Im}(\mathcal{Z}^{Q_1,d}) = -\mathrm{Im}(\mathcal{Z}^{Q_3,d}), \\ \mathrm{Im}(\mathcal{Z}^{Q_2,d}) = -\mathrm{Im}(\mathcal{Z}^{Q_4,d}). \end{cases} \tag{75}$$

Hence, looking at Eq. (65), it can be seen that schemes with $\alpha_1 = \alpha_3$ and $\alpha_2 = \alpha_4$ provide no spurious dispersion, namely, their Fourier footprints lie on the real axis of the complex plane. Thus a one-parameter class of dispersion-free $\mathcal{RD}$ schemes is obtained. Analyzing the expression of the elemental Fourier footprints, Eq. (64), it can be verified that within this class, the only scheme that does not produce amplified modes is the centred one ($\alpha_i = 1/4$, $i = 1, \ldots, 4$). Therefore, the schemes satisfying Eq. (73), with $\psi \neq 0$, provide amplified modes when discretizing the diffusion term.

From the considerations above and the conclusions drawn in Section 4.3, it appears that an appropriate scheme for discretizing the advection–diffusion equation with second-order accuracy on a nine-point stencil would be a hybrid one using the Opt and $\mathcal{FE}$-*Gal* schemes for the advection and diffusion terms, respectively. In fact, the analysis shows that, within the class of second-order accurate schemes for the pure advection operator, $\mathcal{RD}$ $\mathcal{LP}$ schemes, including multidimensional upwind ones, are unsuitable for discretizing diffusion dominated problems since they: (i) provide amplified (or at least undamped) modes arising from the distribution of the diffusive fluctuation; (ii) produce first-order accurate solutions when employed to distribute the convective fluctuation in conjunction with any other discretization scheme for the diffusion term. On the other hand, for advection dominated problems, it could be worth distributing the entire fluctuation according to an upwind $\mathcal{RD}$ $\mathcal{LP}$ approach, since the dissipation introduced by the discretization of the convective term effectively stabilizes the aforementioned undamped modes arising from the diffusion term.

6. Numerical results

6.1. Advection equation

6.1.1. Accuracy study

The accuracy of some $\mathcal{RD}$ schemes for quadrilateral cells has been verified numerically by performing a mesh-refinement study for the linear advection of the sinusoidal profile,

$$u = \cos\left[\pi\left(y - \frac{b}{a}x\right)\right],$$

in the domain $[0, 1]^2$, with $\boldsymbol{\lambda} = (a, b)$, $a = 1$, $b = 2$ (solution imposed at inlet boundaries). Four grids have been used, composed of 32^2, 64^2, 128^2, and 256^2 elements, respectively, the second one being shown in Fig. 27. The size of the mesh, namely, the square of the area of the domain divided by the number of elements, is again indicated with h. The logarithms of the L_1, L_2, and L_∞ norms of the errors have been computed and the results are plotted versus the logarithm of h in Figs. 28–32, for the *N*, *PSI*, *LDA*, Opt-AD, and *SUPG* schemes: the *N* scheme, which is not linearity preserving, is only first-order accurate; the *PSI* scheme has an order of accuracy between one and two, as already known [3]; the *LDA*, Opt-AD, and *SUPG* schemes are all seen to be second-order accurate. It is noteworthy that: the results of the *LDA*-AD scheme coincide with those of the *LDA* scheme, within plotting accuracy; the Opt scheme does not converge, as anticipated; the *SUPG* scheme is third-order accurate when using a uniform Cartesian grid, as shown in Fig. 33, provided here for completeness. Furthermore, Fig. 34 provides a comparison among the convergence histories of the various schemes, using an explicit Euler time integration and the non Cartesian grid with 32^2 elements. The *SUPG* scheme requires the minimum number of iterations among the second-order accurate ones. The addition of the artificial dissipation term slightly improves the performance of the *LDA* scheme, somewhat alleviating the problems due to the marginal stability of $\mathcal{LP}$ schemes for high-frequency

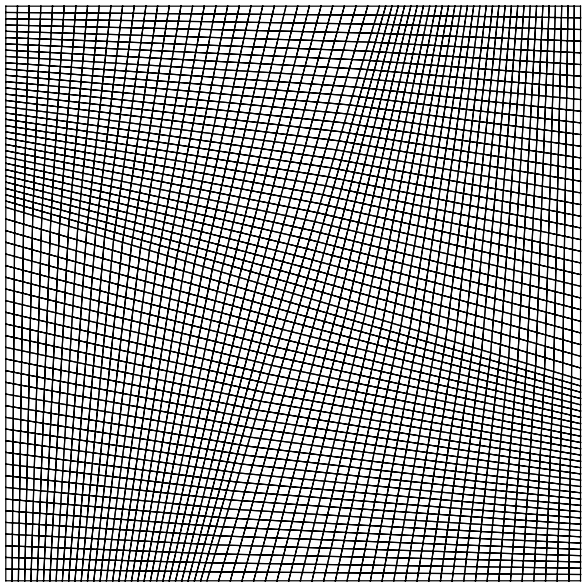

Fig. 27. Non Cartesian 64^2 grid used for the accuracy study.

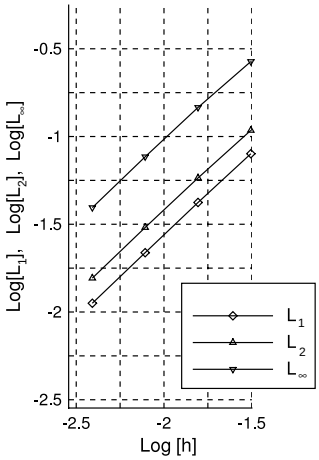

Fig. 28. Accuracy study for the N scheme.

modes. The Opt-AD scheme is the slowest second-order accurate one. Finally, the *PSI* scheme is the worst performing one, due to its non-linearity. Notice that the CPU time required by each iteration of the *SUPG* scheme is about equal to that needed for three iterations of either the Opt-AD or *LDA*-AD scheme, and ten iterations of the LDA scheme, which, for the present case, turns out to be the most efficient second-order accurate scheme.

6.1.2. Discontinuous solutions

The performance of $\mathcal{RD}$ schemes in the presence of discontinuities and for the case of non-linear advection have been addressed for completeness.

The convection of a discontinuous profile with $\boldsymbol{\lambda} = (a, b)$, $a = 2$, $b = 1$ has been computed in the domain $\Omega = [0, 1]^2$, discretized by the 32^2 non-Cartesian mesh of Fig. 35. The boundary conditions are: $u(x, y = 0) = 3$, $u(x = 0, y) = 5$, and $u(x = 0, y = 0) = 4$. The numerical results are presented in Fig. 36. As expected, the N and *PSI* schemes yield monotone solutions, the first one being markedly more diffusive,

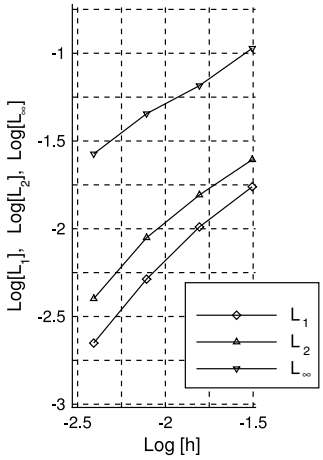

Fig. 29. Accuracy study for the *PSI* scheme.

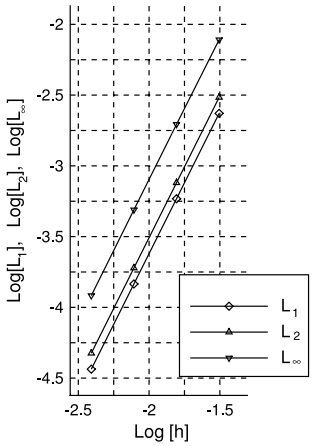

Fig. 30. Accuracy study for the *LDA* scheme.

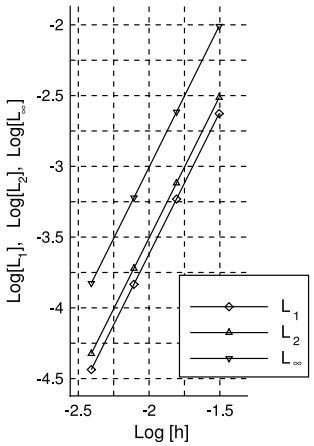

Fig. 31. Accuracy study for the Opt-AD scheme.

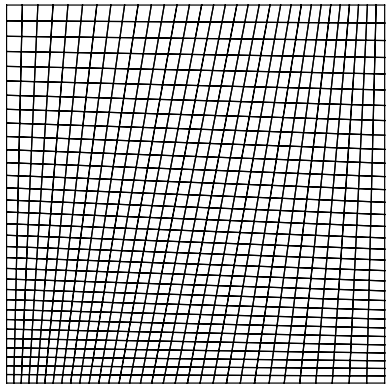

Fig. 35. Non Cartesian grid for the computation of discontinuous solutions.

whereas the solutions obtained using the *LDA* scheme is affected by spurious oscillations, which are reduced by the AD bias common to the *SUPG*, *LDA*-AD, and Opt-AD schemes. In order to provide a more precise comparison of the performance of these schemes, Fig. 37 shows their solutions at $y = 1$. The *PSI* scheme is clearly the most suitable one for computing discontinuous solutions; the *LDA*-TR (*LDA* scheme on an unstructured triangular grid with 32 elements on the boundaries), *SUPG*, *LDA*-AD, and Opt-AD schemes are just about equivalent and superior to the *LDA* one.

Furthermore, Burgers' equation has been solved on the domain $\Omega = [0, 1]^2$, with boundary conditions: $u(x, y = 0) = 1.5 - 2x$, $u(x = 0, y) = 1.5$, and $u(x = 1, y) = -0.5$. The cell-linearized advection velocity used to compute the inflow parameters is evaluated as the arithmetic average of the nodal values. The solutions obtained using again the grid of Fig. 35 are provided in Fig. 38. Like in the previous test-case, the *N* and *PSI* schemes yield monotone solutions, whereas the *LDA*, *LDA*-AD, *SUPG*, and Opt-AD schemes produce spurious oscillations. Finally, Fig. 39 provides the solutions at $y = 0.25$ and $y = 0.75$ for the *SUPG*, Opt-AD, and *PSI* schemes. The three solutions are equivalent in the fan region, whereas the *PSI* scheme is again the best one for computing the discontinuity.

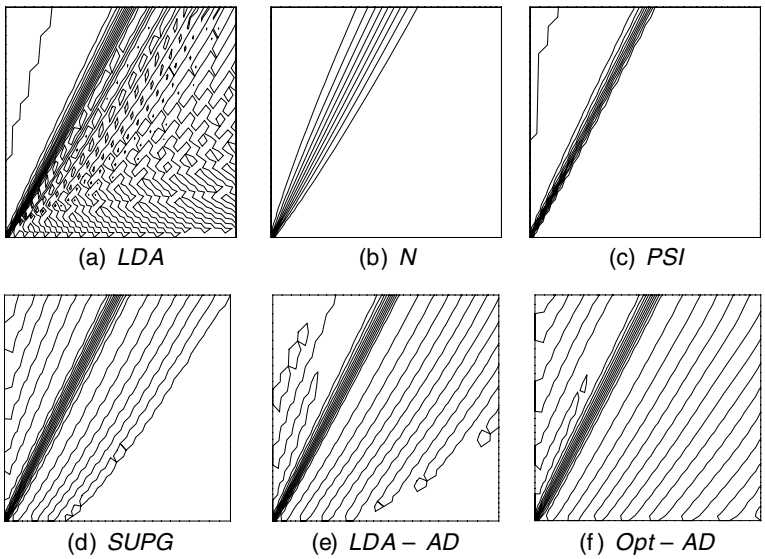

Fig. 36. Advection of a step: contour lines from $u = 3$ to $u = 6$ with spacing $\Delta u = 0.2$.

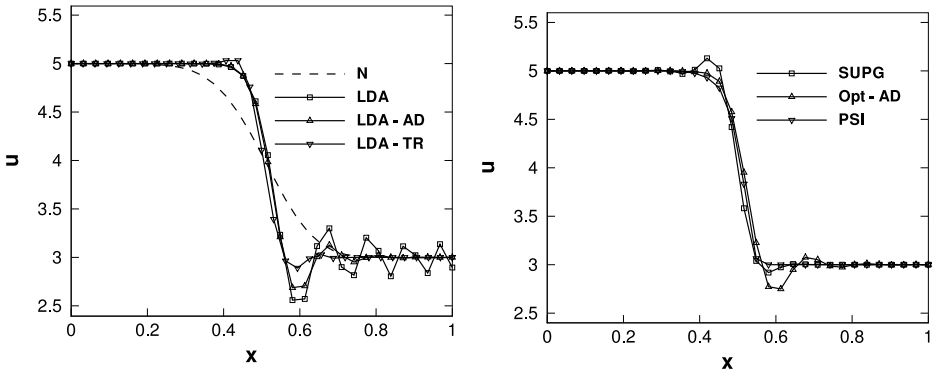

Fig. 37. Advection of a step: cut of the solution at $y = 1$, for the *N*, *LDA*, *LDA*-AD, and *LDA*-TR schemes (left) and for the *SUPG*, Opt-AD, and *PSI* schemes (right).

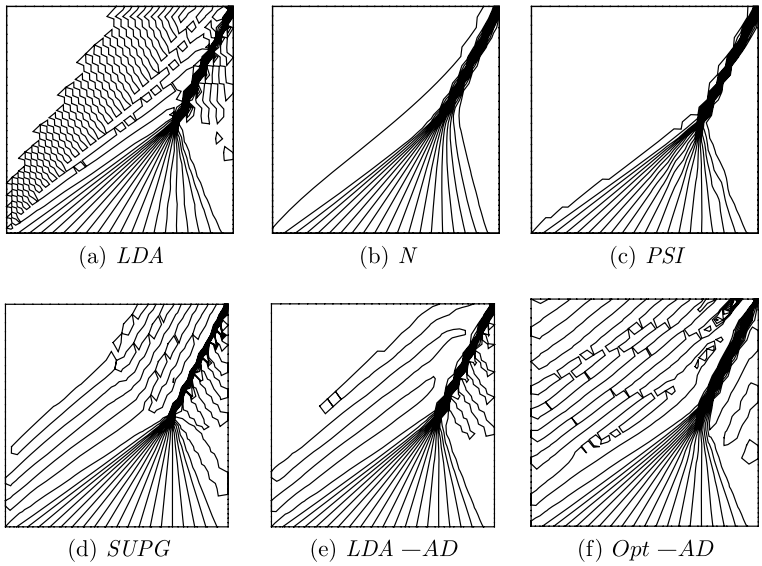

(a) *LDA* (b) *N* (c) *PSI*

(d) *SUPG* (e) *LDA —AD* (f) *Opt —AD*

Fig. 38. Burgers' equation: contour lines from $u = -0.5$ to $u = 2.5$ with spacing $\Delta u = 0.1$.

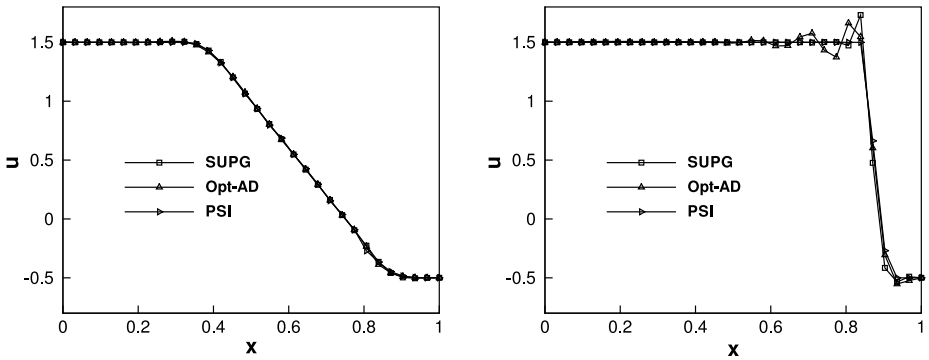

(a) solution cut at $y = 0.25$ (b) solution cut at $y = 0.75$

Fig. 39. Burgers' equation: cut of the solution with the *SUPG*, Opt-AD, and *PSI* schemes at $y = 0.25$ and at $y = 0.75$.

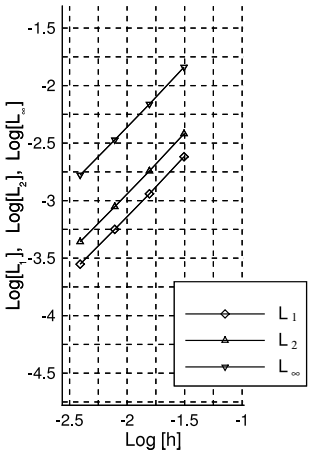

Fig. 40. Accuracy study for the hybrid *LDA-$\mathcal{FE}$* approach.

6.2. Advection–diffusion equation

The advection–diffusion problem used in [26] has been considered as a suitable problem for testing the accuracy of the considered schemes. The linear advection–diffusion equation is solved in the domain $[0, 1]^2$, with boundary conditions such that the following exact solution holds:

$$u = -\cos(2\pi k\eta)\exp\left[\frac{1}{2}\xi\frac{1-\sqrt{1+16\pi^2k^2\mu^2}}{\mu}\right],$$

where $\xi = ax + by$ and $\eta = bx - ay$. The computations have been performed with $\boldsymbol{\lambda} = (a, b)$, $a = 1$, $b = 2$, $\mu = 0.1$, and two solution frequencies, namely, $k = 1$ and $k = 4$.

Four grids have been used with 32^2, 64^2, 128^2, and 256^2 elements, respectively, the coarsest one being shown in Fig. 35. Firstly, two approaches have been tested, namely, the hybrid one using the *LDA* and *$\mathcal{FE}$-Gal* schemes (*LDA-$\mathcal{FE}$*) and the residual-based approach using the *LDA* scheme for both the advective and diffusive fluctuations (*LDA–LDA*). The logarithms of the L_1, L_2, and L_∞ norms of the errors obtained using $k = 1$ are plotted versus the logarithm of h in Figs. 40 and 41, respectively. The hybrid $LDA - \mathcal{FE}$ approach is only first-order accurate, whereas the $\mathcal{LP}$ *LDA–LDA* scheme ensures second-order accuracy. However, the latter

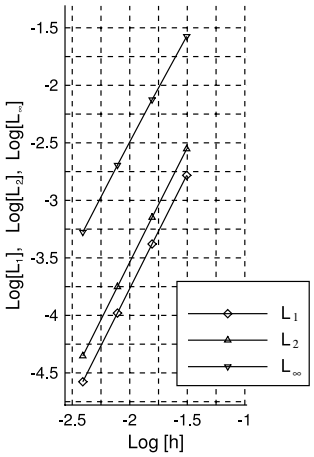

Fig. 41. Accuracy study for the *LDA–LDA* scheme.

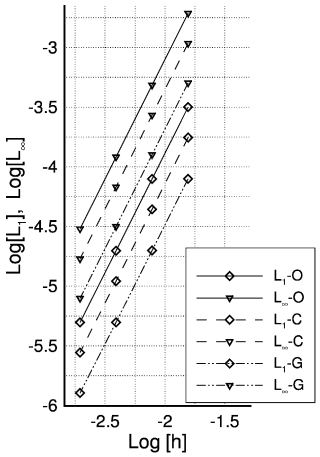

Fig. 42. Accuracy study: uniform Cartesian grid and $k = 1$.

approach is characterized by a marginal stability for the high-frequency modes, which remarkably slows down convergence for finer grids (lower *Pe*), see Fig. 48.

Then, two dissipation-free hybrid approaches have been considered, using the $\mathcal{FE}$-*Gal* scheme for the diffusion term and either the centred or the Opt $\mathcal{RD}$ scheme for the advection term. These schemes, denoted here as C and O, respectively, have been used on four uniform Cartesian grids with 64^2, 128^2, 256^2 and 512^2 elements: the logarithms of the norms of the solution errors are shown in Figs. 42 and 43 for $k = 1$ and $k = 4$, respectively. The results obtained using the $\mathcal{FE}$-*Gal* scheme for the entire residual (labeled G) are also shown, for comparison. For $k = 1$, the errors of the G scheme are the smallest ones, those of the C scheme being smaller than those of the O one. For $k = 4$, the O scheme is seen to outperform both the G and C ones. These results are not surprising insofar as, for a single mode, the O scheme can be either superior or inferior to the other ones; however, it is anticipated that for the general case of a solution with a wide frequency spectrum, the O scheme would perform best, insofar as the Opt scheme has been designed by minimizing the error over the entire range of frequencies.

Then, solutions have been obtained on four non uniform grids with 64^2, 128^2, 256^2 and 512^2 elements, similar to the one in Fig. 35, and the logarithms of the error norms for $k = 1$ and $k = 4$ are shown in Figs. 44 and 45, respectively. The three schemes appear to be second-order accurate also on these non uniform grids, their differences remaining similar with respect to the case of uniform Cartesian grids. For completeness, the

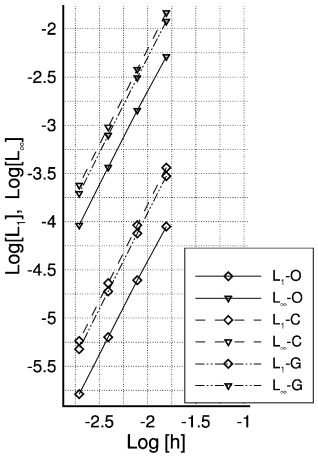

Fig. 43. Accuracy study: uniform Cartesian grid and $k = 4$.

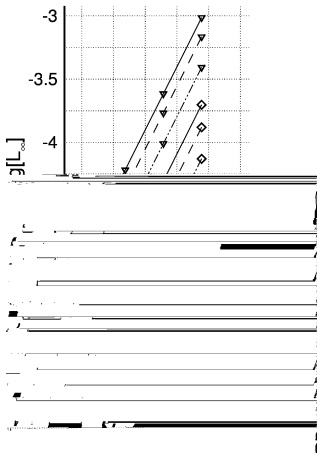

Fig. 44. Accuracy study: non Cartesian grid and $k = 1$.

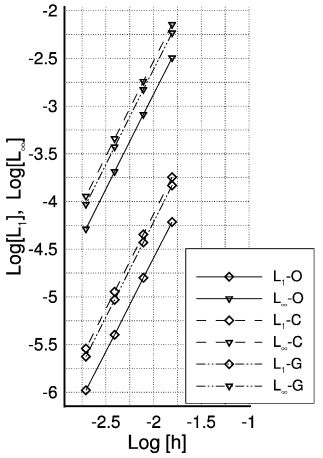

Fig. 45. Accuracy study: non Cartesian grid and $k = 4$.

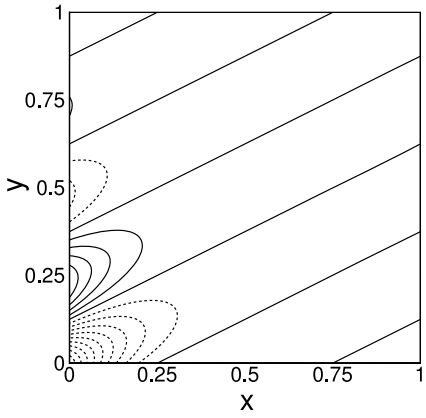

Fig. 46. Advection–diffusion problem: solution contours for $k = 1$ using the O scheme.

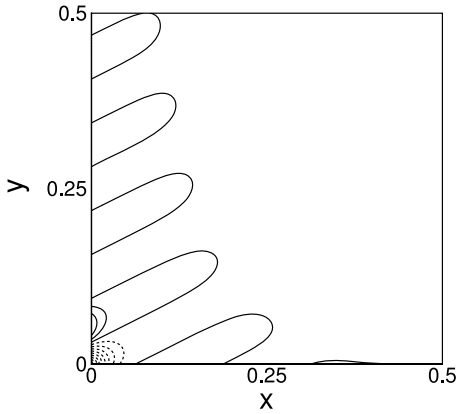

Fig. 47. Advection–diffusion problem: solution contours for $k = 4$ using the O scheme.

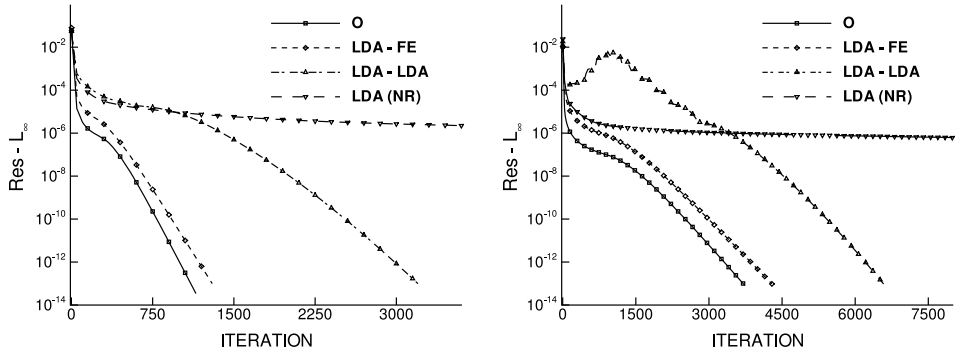

Fig. 48. Convergence history to steady state for the advection–diffusion problem on grids with 32^2 (left, $Pe \approx 0.69$) and 64^2 (right, $Pe \approx 0.35$) elements.

contour lines of the solutions obtained using the O scheme on the 128^2 grid are given in Figs. 46 and 47 for $k = 1$ and $k = 4$, respectively.

Finally, in order to verify the results of Section 4.3 about discretizations based on $\mathcal{LP}$ schemes either to distribute the entire residual or using a hybrid approach, computations have been performed using also the *LDA-*$\mathcal{FE}$ and *LDA–LDA* schemes, as well as the blended scheme of Nishikawa and Roe [26] (indicated as *LDA*(NR)). For the case $k = 1$, the convergence histories obtained on two grids with 32^2 and 64^2 elements, corresponding to $Pe \approx 0.69$ and $Pe \approx 0.35$, are shown in Fig. 48 together with those of the O scheme. The O scheme is seen to converge to steady-state faster than the other ones, insofar as it does not produce

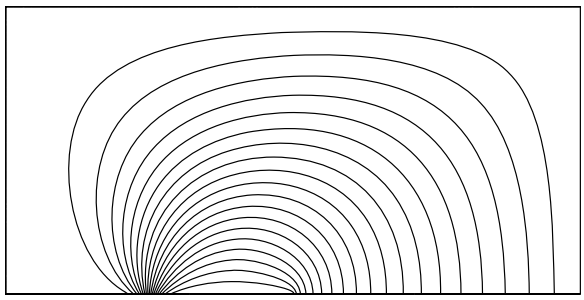

Fig. 49. Smith and Hutton problem: reference solution on the 512×256 grid with $\mu = 0.1$.

undamped modes, like the C and G schemes, which experience very similar convergence histories (not shown in the figure). The *LDA*(NR) scheme is very slow to converge (machine zero is achieved in about 80,000 iterations on the 64^2 grid) due to some marginally stable modes. The *LDA–LDA* scheme is characterized by some unstable modes associated with the discretization of the diffusion term. For the considered meshes, such modes are stabilized by the numerical dissipation due to the discretization of the convective term, but if h (Pe) is reduced further, the calculation eventually becomes unstable. It is noteworthy that, for the finer, but still rather coarse 64^2 mesh, these unstable modes produce an initial increase of the residual, as shown in Fig. 48 (right).

A final test-case has been considered, namely, the scalar advection–diffusion of a steep gradient proposed by Smith and Hutton [29]. Computations have been performed in the domain $[-1, 1]\times[0, 1]$ with $\boldsymbol{\lambda} = (a, b)$, $a = 2y(1 - x^2)$, $b = -2x(1 - y^2)$. The following boundary conditions are imposed:

$$u(x, 0) = 1 + \tanh(20x + 10) \quad \text{at } -1 \leqslant x \leqslant 0 \text{ (inlet boundary)};$$

$$\frac{\partial u(x, 0)}{\partial y} = 0 \quad \text{at } 0 < x \leqslant 1 \text{ (outlet boundary)};$$

$$u(x, y) = 1 - \tanh 10 \quad \text{at the other boundaries.}$$

Two cases have been considered with $\mu = 0.1$ and 0.001, respectively, using a uniform Cartesian grid with 32×16 elements. The reference solution contours, computed on a 512×256 grid using the O scheme, are shown in Figs. 49 and 50, respectively. Figs. 51 and 52 provide the distributions of the solutions along the outlet boundary, obtained employing several schemes together with the reference solution for $\mu = 0.1$ and $\mu = 0.001$, respectively. For the first case, which represents an advection–diffusion problem with $Pe \simeq 1$, it appears that: the C, O, and G schemes provide similar, satisfactory solutions; the *LDA-FE* and *SUPG-FE* schemes provide similar, less satisfactory results; the LDA–LDA and LDA(NR) schemes provide unsatisfactory solu-

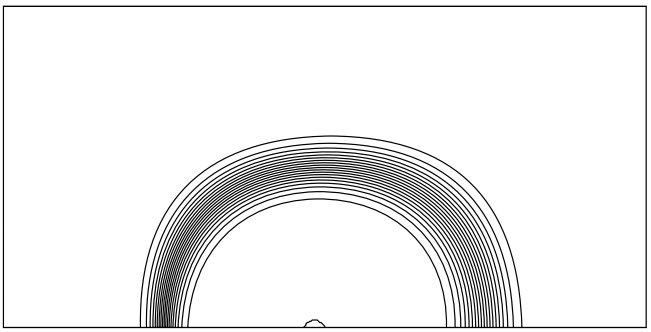

Fig. 50. Smith and Hutton problem: reference solution on the 512×256 grid with $\mu = 0.001$.

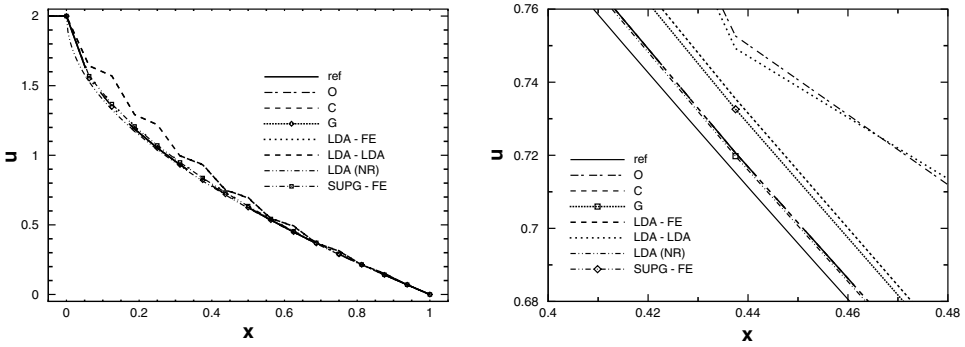

Fig. 51. Smith and Hutton problem: solution along the entire outlet boundary for $\mu = 0.1$ on a 32×16 grid (left); local view (right).

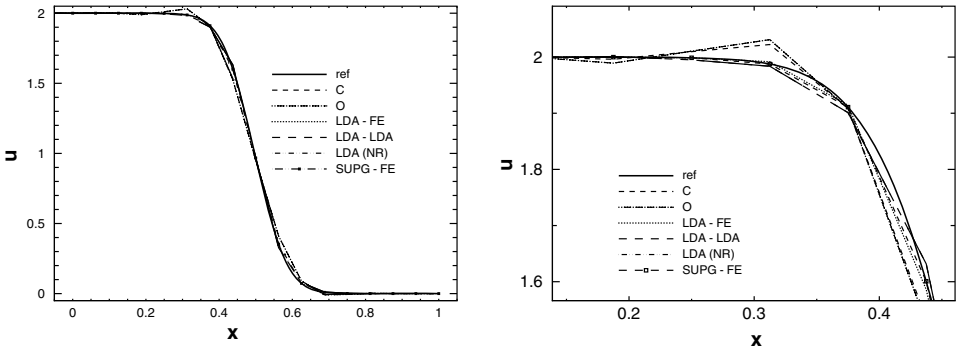

Fig. 52. Smith an Hutton problem: solution along the entire outlet boundary for $\mu = 0.001$ on a 32×16 grid (left); partial view (right).

tions. For the second case, which represents an advection dominated problem with $Pe \simeq 100$, the artificial dissipation term had to be added to the C and O schemes to ensure convergence; nevertheless, some spurious oscillations are still present in their solutions. On the other hand, the *SUPG-$\mathcal{FE}$* scheme is seen to provide a very accurate solution and the LDA–LDA and LDA(NR) schemes are quite satisfactory.

7. Conclusions

This paper has presented a theoretical and numerical analysis of some difficulties arising when extending residual distribution schemes for scalar advection and advection–diffusion problems from triangular grids to quadrilateral ones. In particular, a multidimensional spectral analysis is provided, which enables one to analyze all grid-resolved two-dimensional Fourier modes for a given advection angle. A two-dimensional generalization of the modified wavenumber definition is proposed, which provides a general framework for the multidimensional analysis and comparison of different schemes.

Concerning the discretization of the convective term, the performance of the most successful second-order accurate fluctuation splitting schemes, originally designed for triangles, have been assessed when applied to bilinear quadrilateral cells. Moreover, a scheme with minimum dispersion-error on a nine-point stencil has been designed, having zero dissipation, and an *SUPG* scheme for quadrilaterals is derived, which is third-order accurate for uniform Cartesian grids and second-order accurate for general quadrilaterals. Linearity preserving schemes (such as the *LDA* and Lax–Wendroff schemes) are shown to provide lower dissipation with respect to their triangle-based counterparts, and low or no damping for high frequency Fourier modes. Moreover, it has been proven that this property is shared by any linearity preserving scheme on quadrilaterals, which, therefore, cannot be employed in practical computations for pure advection problems, without adding some artificial dissipation to damp marginally stable modes. In this paper, $\mathcal{LP}$ schemes are stabilized effectively by the bias term of the *SUPG* scheme, which does not lower their order of accuracy while preserving the compactness of the scheme.

Concerning the discretization of the advection–diffusion equation, the analysis demonstrates that: (i) using a hybrid approach, which employs an upwind residual distribution scheme for the convective fluctuation and any other scheme for the diffusion term, leads to a first-order accurate method, as already shown by Nishikawa and Roe for the case of triangular grids; (ii) distributing the entire residual by an upwind approach provides a second-order accurate scheme, which is unstable for diffusion dominated problems, due to the undamped modes stemming from the splitting of the diffusive fluctuation. For advection dominated problems, the dissipation introduced by the upwind treatment of the convective term could be effective to stabilize the undamped modes arising from the diffusion term. However, even the blended approach of Nishikawa and Roe, which smoothly varies the distribution coefficients from an upwind scheme, for high (numerical) Peclet numbers, to a centred one, for low Peclet numbers still provides marginally stable modes. Starting from this scenario, the conditions for a hybrid approach to be second-order accurate have been obtained and a suitable discretization of the advection–diffusion equation has been proposed, employing the minimum-dispersion-error scheme for the convective term and the $\mathcal{FE}$ Galerkin scheme for the diffusion one. The dissipation

and dispersion properties of such a discretization have been compared with those of the state-of-the-art schemes having the same computational molecule. Several test-cases for linear and non-linear advection problems as well as linear advection–diffusion problems have been used to confirm and supplement the theoretical findings by numerical experiments.

Appendix A. Finite difference expression of schemes

A.1. Advection operator

In this section the finite difference expressions of the schemes of interest are provided, using the notation of Fig. 3.

- N scheme ($\delta \in [0, \pi/4]$):

$$(\boldsymbol{\lambda}\cdot\nabla u)_i^N \simeq \frac{\|\boldsymbol{\lambda}\|}{4h}[4(u_q-u_i)\cos(\delta)+(u_j+u_p-2u_q)\sec(\delta)+2(u_j-u_p)\sin(\delta)]. \tag{A.1}$$

- Generic $\mathcal{LP}$ scheme on the uniform $P1$ triangulation of Fig. 4:

$$\begin{aligned}(\boldsymbol{\lambda}\cdot\nabla u)_i^{\mathcal{LP}} \simeq \frac{\|\boldsymbol{\lambda}\|}{2h}[&\cos(\delta)((u_q-u_i)\gamma_1+(u_j-u_k)\gamma_2+(u_i-u_m)(\gamma_3+\gamma_4)+(u_o-u_n)\gamma_5-(u_i-u_q)\gamma_6)\\ &+\sin(\delta)((u_j-u_q)\gamma_1+(u_k-u_i)\gamma_2+(u_k-u_i)\gamma_3+(u_m-u_n)\gamma_4+(u_i-u_o)(\gamma_5+\gamma_6))].\end{aligned} \tag{A.2}$$

- Generic $\mathcal{LP}$ scheme on $Q1$ quadrilaterals:

$$\begin{aligned}(\boldsymbol{\lambda}\cdot\nabla u)_i^{\mathcal{LP}} \simeq{}& \frac{\|\boldsymbol{\lambda}\|}{2h}\cos(\delta)[(-u_i+u_j-u_k+u_q)\gamma_1+(u_i+u_k-u_l-u_m)\gamma_2+(u_i-u_m-u_n+u_o)\gamma_3\\ &-(u_i+u_o-u_p-u_q)\gamma_4]+\frac{\|\boldsymbol{\lambda}\|}{2h}\sin(\delta)[(-u_i+u_j+u_k-u_q)\gamma_1+(-u_i+u_k+u_l-u_m)\gamma_2\\ &+(u_i+u_m-u_n-u_o)\gamma_3+(u_i-u_o-u_p+u_q)\gamma_4].\end{aligned} \tag{A.3}$$

For completeness, the distribution coefficients[1] are given for the LDA scheme (with $\delta \in (0, \pi/4)$):

$$\gamma_1=\frac{1+\tan(\delta)}{2},\quad \gamma_2=\gamma_3=0,\quad \gamma_4=\frac{1-\tan(\delta)}{2}, \tag{A.4}$$

and for the LW scheme (which coincides with Ni's LW scheme):

$$\begin{aligned}\gamma_1&=\frac{1}{4}\left[1+\frac{\|\boldsymbol{\lambda}\|\Delta t}{\Delta x}(\sin(\delta)+\cos(\delta))\right],\\ \gamma_2&=\frac{1}{4}\left[1-\frac{\|\boldsymbol{\lambda}\|\Delta t}{\Delta x}(\sin(\delta)-\cos(\delta))\right],\\ \gamma_3&=\frac{1}{4}\left[1-\frac{\|\boldsymbol{\lambda}\|\Delta t}{\Delta x}(\sin(\delta)+\cos(\delta))\right],\\ \gamma_4&=\frac{1}{4}\left[1+\frac{\|\boldsymbol{\lambda}\|\Delta t}{\Delta x}(\sin(\delta)-\cos(\delta))\right].\end{aligned} \tag{A.5}$$

- $SUPG$ scheme:

$$\begin{aligned}(\boldsymbol{\lambda}\cdot\nabla u)_i^{SUPG} \simeq \frac{\|\boldsymbol{\lambda}\|}{12h}[&-8u_i+u_j+u_k+u_l+u_m+u_n+u_o+u_p+u_q+3\cos(2\delta)(-u_k+u_m-u_o+u_q)\\ &+\sin(\delta)(u_j+4u_k+u_l-u_n-4u_o-u_p)+\cos(\delta)(u_j-u_l-4u_m-u_n+u_p+4u_q\\ &+3\sin(\delta)(u_j-u_l+u_n-u_p))].\end{aligned} \tag{A.6}$$

[1] Counterclockwise vertex numbering starting from the left bottom one.

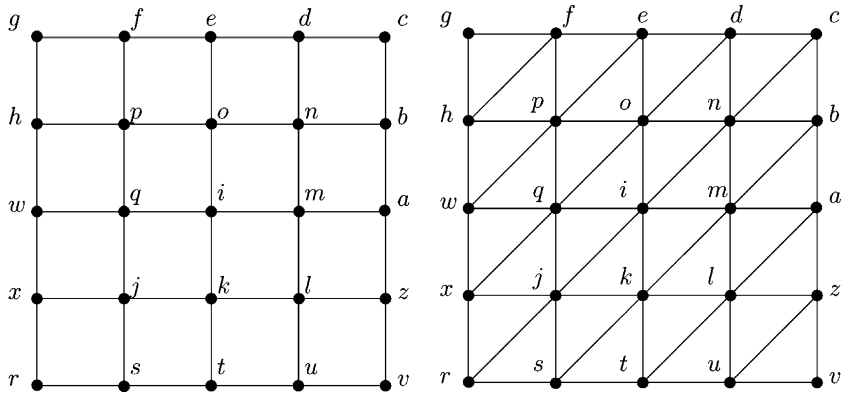

Fig. A.1. Notation for the diffusion operators on quadrilateral and triangular cells.

- Second-order accurate (fully) upwind $\mathcal{FD}$ scheme (with $\delta \in (0, \pi/2)$:

$$(\boldsymbol{\lambda}\cdot\nabla u)_i^{\mathcal{FD}\text{-upw2}} \simeq \frac{\|\boldsymbol{\lambda}\|}{2h}[\cos(\delta)(3u_i - 4u_q + u_w) + \sin(\delta)(3u_i - 4u_k + u_t)]. \tag{A.7}$$

A.2. Diffusion operator

In this section the finite difference expressions of the schemes of interest are provided, using the notation of Fig. A.1.

- $\mathcal{LP}$ scheme on triangles:

$$\begin{aligned}-(\mu\nabla^2 u)_i^{\mathcal{LP}} \simeq \frac{\mu}{12h^2}[&(-4u_i - 4u_j + 2u_k + 2u_m + u_n - u_o + 3u_p - 4u_q + u_r + 2u_s + 3u_w - u_x)\alpha_1\\ &+ (4u_i + 4u_j + 4u_k - 3u_l + u_m - u_n - 2u_o - 2u_q - u_r + u_s - 3u_t - 2u_x)\alpha_2\\ &+ (2u_a + u_b - 4u_i - u_j - 4u_k + 2u_l - 4u_m - u_n + 3u_o + 3u_q + u_s + 2u_t)\alpha_3\\ &+ (3u_a - u_b + u_c + 2u_d - 4u_i + u_j - u_k + 3u_l + 2(-2u_m - 2u_n + u_o + u_q))\alpha_4\\ &+ (2u_b + u_c - u_d + 3u_e - 4u_i + u_j + 2u_k + 2u_m - 4u_n - 4u_o + 3u_p - u_q)\alpha_5\\ &+ (u_d + 2u_e - 4u_i - u_j + 3u_k + 3u_m - u_n - 4u_o + 2(u_p - 2u_q + u_w) + u_x)\alpha_6].\end{aligned} \tag{A.8}$$

- $\mathcal{LP}$ scheme on quadrilaterals

$$\begin{aligned}-(\mu\nabla^2 u)_i^{\mathcal{LP}} \simeq \frac{\mu}{4h^2}[&(-2u_i - 2u_j - 2u_k + u_l + u_m + u_o + u_p - 2u_q + u_s + u_t + u_w + u_x)\alpha_1\\ &+ (u_a - 2u_i + u_j - 2u_k - 2u_l - 2u_m + u_n + u_o + u_q + u_t + u_u + u_z)\alpha_2\\ &+ (u_a + u_b + u_d + u_e - 2u_i + u_k + u_l - 2u_m - 2u_n - 2u_o + u_p + u_q)\alpha_3\\ &+ (u_e + u_f + u_h - 2u_i + u_j + u_k + u_m + u_n - 2(u_o + u_p + u_q) + u_w)\alpha_4].\end{aligned} \tag{A.9}$$

- $\mathcal{FE}$-*Gal* scheme on triangles:

$$-(\mu\nabla^2 u)_i^{\mathcal{FE}-Gal} \simeq \frac{\mu}{h^2}(-4u_i + u_k + u_q + u_m + u_o). \tag{A.10}$$

note that in this particular configuration this discretization coincides with the second-order accurate centred $\mathcal{FD}$ scheme;

- $\mathcal{FE}$-*Gal* scheme on quadrilaterals:

$$-(\mu\nabla^2 u)_i^{\mathcal{FE}-Gal} \simeq \frac{\mu}{3h^2}(-8u_i + u_j + u_k + u_l + u_m + u_n + u_o + u_p + u_q). \tag{A.11}$$

Appendix B. Fourier analysis: advection operator

In this section the expressions of the real part of the Fourier footprint, $\mathrm{Re}(\mathcal{Z})$, and of the modified wavenumber, $\mathrm{Re}(\tilde{\beta}')$, are provided as functions of δ, β_x, and β_y.

B.1. Dissipative properties: $\mathrm{Re}(\mathcal{Z})$

- First-order accurate $\mathcal{FD}$ upwind scheme:

$$\mathrm{Re}(\mathcal{Z}) = (\cos(\beta_x) - 1)\cos(\delta) + (\cos(\beta_y) - 1)\sin(\delta). \tag{B.1}$$

- Second-order accurate $\mathcal{FD}$ (fully) upwind scheme:

$$\mathrm{Re}(\mathcal{Z}) = -4\left[\cos(\delta)\sin^4\left(\frac{\beta_x}{2}\right) + \sin^4\left(\frac{\beta_y}{2}\right)\sin(\delta)\right]. \tag{B.2}$$

- N scheme on quadrilaterals:

$$\mathrm{Re}(\mathcal{Z}) = \frac{1}{2}(2(\cos(\beta_x) - 1)\cos(\delta) + \cos(\beta_x)(\cos(\beta_y) - 1)\sec(\delta) - 2\sin(\beta_x)\sin(\beta_y)\sin(\delta)). \tag{B.3}$$

- LDA scheme on quadrilaterals:

$$\mathrm{Re}(\mathcal{Z}) = 2[(\cos(\beta_x)\cos(\beta_y) + (\cos(\beta_x) - \cos(\beta_y))\cos(2\delta) - 1)\sec(\delta) - 2\sin(\beta_x)\sin(\beta_y)\sin(\delta)]. \tag{B.4}$$

- LW scheme on quadrilaterals:

$$\mathrm{Re}(\mathcal{Z}) = \frac{1}{2}[\cos(\beta_x)\cos(\beta_y) + (\cos(\beta_x) - \cos(\beta_y))\cos(2\delta) - 2\cos(\delta)\sin(\beta_x)\sin(\beta_y)\sin(\delta) - 1]. \tag{B.5}$$

- $SUPG$ scheme on quadrilaterals (same as all non-dissipative $\mathcal{LP}$ schemes stabilized with the addition of artificial dissipation):

$$\begin{aligned}\mathrm{Re}(\mathcal{Z}) = &\frac{1}{6}[\cos(\beta_y) + \cos(\beta_x)(2\cos(\beta_y) + 1) + 3(\cos(\beta_x) - \cos(\beta_y))\cos(2\delta)\\ &- 3\sin(\beta_x)\sin(\beta_y)\sin(2\delta) - 4].\end{aligned} \tag{B.6}$$

- N scheme on triangles:

$$\mathrm{Re}(\mathcal{Z}) = (\cos(\beta_x) - 1)\cos(\delta) + (\cos(\beta_x + \beta_y) - \cos(\beta_x))\sin(\delta). \tag{B.7}$$

- LDA scheme on triangles:

$$\mathrm{Re}(\mathcal{Z}) = \frac{1}{2}[-2\sec(\delta) + 2\cos(\beta_x)(\cos(\delta) - \sin(\delta)) + 2\sin(\delta)(\cos(\beta_x + \beta_y) + \cos(\beta_y)(\tan(\delta) - 1) + 1)]. \tag{B.8}$$

- LW scheme on triangles:

$$\mathrm{Re}(\mathcal{Z}) = \cos(\beta_x)\cos^2(\delta) + \cos(\beta_y)\sin^2(\delta) + \sin\left(\frac{\beta_y}{2}\right)\left(\sin\left(\frac{\beta_y}{2}\right) - \sin\left(\beta_x + \frac{\beta_y}{2}\right)\right)\sin(2\delta) - 1. \tag{B.9}$$

B.2. Dispersive properties: $\mathrm{Re}(\tilde{\beta}')$

- First-order accurate upwind $\mathcal{FD}$ scheme and second-order accurate centred $\mathcal{FD}$ scheme:

$$\mathrm{Re}(\tilde{\beta}') = \cos(\delta)\sin(\beta_x) + \sin(\beta_y)\sin(\delta). \tag{B.10}$$

- $\mathcal{FE}$-Gal scheme on quadrilaterals (same as fourth-order accurate centred scheme of [24] on uniform Cartesian setting) and $SUPG$ scheme:

$$\mathrm{Re}(\tilde{\beta}') = \frac{1}{3}((\cos(\beta_y)+2)\cos(\delta)\sin(\beta_x) + (\cos(\beta_x)+2)\sin(\beta_y)\sin(\delta)). \tag{B.11}$$

- Second-order accurate (fully) upwind $\mathcal{FD}$ scheme:

$$\mathrm{Re}(\tilde{\beta}') = (2-\cos(\beta_x))\cos(\delta)\sin(\beta_x) + (2-\cos(\beta_y))\sin(\beta_y)\sin(\delta). \tag{B.12}$$

- N and LDA scheme on quadrilaterals:

$$\mathrm{Re}(\tilde{\beta}') = \frac{1}{2}(\cos(\beta_y)+\cos(2\delta))\sec(\delta)\sin(\beta_x) + \cos(\beta_x)\sin(\beta_y)\sin(\delta). \tag{B.13}$$

- LW and centred $\mathcal{RD}$ schemes on quadrilaterals:

$$\mathrm{Re}(\tilde{\beta}') = \sin(\beta_y)\sin(\delta)\cos^2\left(\frac{\beta_x}{2}\right) + \cos^2\left(\frac{\beta_y}{2}\right)\cos(\delta)\sin(\beta_x). \tag{B.14}$$

- Optimal $\mathcal{RD}$ scheme on quadrilaterals:

$$\begin{aligned}\mathrm{Re}(\tilde{\beta}') =& 2\left[\cos\left(\frac{\beta_y}{2}\right)\cos(\delta)\sin\left(\frac{\beta_x}{2}\right) + \cos\left(\frac{\beta_x}{2}\right)\sin\left(\frac{\beta_y}{2}\right)\sin(\delta)\right] \\ &\times\left[\cos\left(\frac{\beta_x-\beta_y}{2}\right) - 4\sin\left(\frac{\beta_x}{2}\right)\sin\left(\frac{\beta_y}{2}\right)\left(\frac{1}{4}+\frac{7}{12}\sin(2\delta)\right)\right].\end{aligned} \tag{B.15}$$

- N and LDA scheme on triangles:

$$\mathrm{Re}(\tilde{\beta}') = \cos(\delta)\sin(\beta_x) + 2\cos\left(\beta_x+\frac{\beta_y}{2}\right)\sin\left(\frac{\beta_y}{2}\right)\sin(\delta). \tag{B.16}$$

- LW and centred $\mathcal{RD}$ schemes on triangles:

$$\mathrm{Re}(\tilde{\beta}') = \frac{1}{3}[\cos(\delta)(2\sin(\beta_x)-\sin(\beta_y)+\sin(\beta_x+\beta_y)) + (-\sin(\beta_x)+2\sin(\beta_y)+\sin(\beta_x+\beta_y))\sin(\delta)]. \tag{B.17}$$

- Compact $\mathcal{FD}$ centred schemes: to this class of schemes belong the approximations of the form (in 1D):

$$\beta u'_{i-2} + \alpha u'_{i-1} + u'_i + \alpha u'_{i+1} + \beta u'_{i+2} = c\frac{u_{i+3}-u_{i-3}}{6h} + b\frac{u_{i+2}-u_{i-2}}{4h} + a\frac{u_{i+1}-u_{i-1}}{2h}; \tag{B.18}$$

which are characterized by the following modified wavenumber in 2D:

$$\mathrm{Re}(\tilde{\beta}') = \cos(\delta)\frac{(6a\sin(\beta_x)+3b\sin(2\beta_x)+2c\sin(3\beta_x))}{6(2\alpha\cos(\beta_x)+2\beta\cos(2\beta_x)+1)} + \sin(\delta)\frac{(6a\sin(\beta_y)+3b\sin(2\beta_y)+2c\sin(3\beta_y))}{6(2\alpha\cos(\beta_y)+2\beta\cos(2\beta_y)+1)}. \tag{B.19}$$

The coefficients corresponding to the fourth-order accurate Padé scheme are:

$$\beta = 0; \quad \alpha = \frac{1}{4}; \quad a = \frac{3}{2}; \quad b = 0; \quad c = 0;$$

whereas the coefficients corresponding to the fourth-order accurate centred $\mathcal{FD}$ scheme are:

$$\alpha = \beta = 0; \quad a = \frac{4}{3}; \quad b = -\frac{1}{3}; \quad c = 0.$$

Appendix C. Fourier analysis: diffusion operator

In this section the expressions of the real part of the Fourier footprint, $\mathrm{Re}(\mathcal{Z})$, are provided as functions of β_x, and β_y.

C.1. Dissipative properties: $\mathrm{Re}(\mathcal{Z})$

- *$\mathcal{FE}$-Gal* discretization on triangles:

$$\mathcal{Z} = 2(\cos(\beta_x) + \cos(\beta_y) - 2). \tag{C.1}$$

- Centred $\mathcal{LP}$ residual based approach on triangles:

$$\begin{aligned}\mathcal{Z} = \frac{1}{18}[&-2\cos(\beta_x) + 5\cos(2\beta_x) + 8\cos(\beta_x - \beta_y) - 2\cos(\beta_y) + 5\cos(2\beta_y) + 2(-4\cos(\beta_x + \beta_y)\\ &+ \cos(2(\beta_x + \beta_y)) + \cos(2\beta_x + \beta_y) + \cos(\beta_x + 2\beta_y) - 6)].\end{aligned} \tag{C.2}$$

- *LDA* $\mathcal{LP}$ residual based approach on triangles:

$$\begin{aligned}\mathrm{Re}(\mathcal{Z}) = \frac{1}{24}[&10\cos(\beta_x - \beta_y) + 4\cos(2\beta_y) - 10\cos(\beta_x + \beta_y) + 2\cos(2(\beta_x + \beta_y)) + 6\cos(\beta_x + 2\beta_y)\\ &- 3\cos(\beta_x - \delta)\sec(\delta) + 5\cos(2\beta_x - \delta)\sec(\delta) + \cos(2\beta_x)(5 - 4\tan(\delta))\\ &+ (2\cos(\beta_x - \beta_y) - 2\cos(\beta_y) + 2\cos(2\beta_y) - 2\cos(\beta_x + \beta_y) + 2\cos(2(\beta_x + \beta_y))\\ &+ 2\cos(2\beta_x + \beta_y) - 4\cos(\beta_x + 2\beta_y) + 3\sin(\beta_x) - 5\sin(2\beta_x))\tan(\delta) + \cos(\beta_x)(4\tan(\delta) - 3) - 16].\end{aligned} \tag{C.3}$$

- *$\mathcal{FE}$-Gal* discretization on quadrilaterals:

$$\mathcal{Z} = \frac{2}{3}(2\cos(\beta_y)\cos(\beta_x) + \cos(\beta_x) + \cos(\beta_y) - 4). \tag{C.4}$$

- Centred $\mathcal{LP}$ residual based approach on quadrilaterals:

$$\mathcal{Z} = 2\cos^2\left(\frac{\beta_x}{2}\right)\cos^2\left(\frac{\beta_y}{2}\right)(\cos(\beta_x) + \cos(\beta_y) - 2). \tag{C.5}$$

- *LDA* $\mathcal{LP}$ residual based approach on quadrilaterals:

$$\mathrm{Re}(\mathcal{Z}) = 2\cos\left(\frac{\beta_x}{2}\right)\cos\left(\frac{\beta_y}{2}\right)(\cos(\beta_x) + \cos(\beta_y) - 2)\left(\cos\left(\frac{\beta_x}{2}\right)\cos\left(\frac{\beta_y}{2}\right) - \sin\left(\frac{\beta_x}{2}\right)\sin\left(\frac{\beta_y}{2}\right)\tan(\delta)\right). \tag{C.6}$$

References

[1] R. Struijs, H. Deconinck, P.L. Roe. Fluctuation Splitting schemes for the 2D Euler equations, in: VKI LS 1991-01, 1991.
[2] P.L. Roe, D. Sidilkover, Optimum positive linear schemes for advection in two and three dimensions, SIAM J. Numer. Anal. 29 (1992) 1542–1588.
[3] H. Paillere, Multidimensional upwind residual distribution schemes for the Euler and Navier–Stokes equations on unstructured grids, PhD thesis, von Karman Institute, 1995.
[4] G.T. Tomaich, A genuinely multi-dimensional upwinding algorithm for the Navier–Stokes equations on unstructured grids using a compact, highly parallelizable spacial discretization, PhD thesis, University of Michigan, 1995.
[5] H. Paillere, J. Boxho, G. Degrez, H. Deconinck, Multidimensional upwind residual distribution schemes for the convection–diffusion equation, Int. J. Numer. Methods Fluids 23 (1996) 923–936.
[6] E. vander Weide, H. Deconinck, E. Issman, G. Degrez, Fluctuation splitting schemes for multidimensional convection problems: an alternative to finite volume and finite element methods, Comput. Mech. 23 (1999) 199–208.
[7] R. Abgrall, Toward the ultimate conservative scheme: following the quest, J. Comput. Phys. 167 (2001) 277–315.
[8] R. Abgrall, M. Mezine, Construction of second-order accurate monotone and stable residual distribution schemes for steady problems, J. Comput. Phys. 195 (2004) 474–507.
[9] P. De Palma, G. Pascazio, G. Rossiello, M. Napolitano, A second-order accurate monotone implicit fluctuation splitting scheme for unsteady problems, J. Comput. Phys. 208 (2004) 1–33.
[10] R.-H. Ni, A multiple grid scheme for solving the Euler equations, AIAA J. 20 (1982) 1565–1572.
[11] K.G. Powell, B. van Leer, A genuinely multi-dimensional upwind cell-vertex scheme for the Euler equations, AIAA Paper 89-0095, 1989.

[12] C.-C Rossow, Accurate solution of the 2-d Euler equations with an efficient cell-vertex upwind scheme, AIAA Paper 93-0071, 1993.
[13] E. van der Weide, H. Deconinck, Fluctuation splitting schemes for the Euler equations, in: K.W. Morton, M.J. Baines (Eds.), Numerical Methods for Fluid Dynamics V, 1996, pp. 623–630.
[14] A. Csík, M. Ricchiuto, H. Deconinck, A conservative formulation of the multidimensional upwind residual distribution schemes for general nonlinear conservation laws, J. Comput. Phys. 179 (2002) 286–312.
[15] T. Quintino, M. Ricchiuto, A. Csík, H. Deconinck, S. Poedts, Conservative multidimensional upwind residual distribution schemes for arbitrary finite elements, in: K. Srinivas, S. Armfield, P. Morgan (Eds.), Computational Fluid Dynamics, Springer Verlag, 2002, pp. 88–93.
[16] H. Deconinck, P.L. Roe, R. Struijs, A multidimensional generalization of Roe's flux difference splitter for the Euler equations, Comput. Fluids 22 (1993) 215–222.
[17] R. Vichnevetsky, J. Bowles, Fourier Analysis of Numerical Approximations of Hyperbolic Equations, SIAM, Philadelphia, 1982.
[18] S.K. Lele, Compact finite difference schemes with spectral-like resolution, J. Comput. Phys. 103 (1992) 16–42.
[19] Y. Li, Wavenumber extended high-order upwind-biased finite-difference schemes for convective scalar transport, J. Comput. Phys. 133 (1997) 235–255.
[20] A. Brooks, T.J.R. Hughes, Streamline upwind Petrov–Galerkin formulations for convection dominated flows with particular emphasis on the incompressible Navier–Stokes equations, Comput. Methods Appl. Mech. Engrg. 32 (1982) 199–259.
[21] P. De Palma, G. Pascazio, D.T. Rubino, M. Napolitano, Residual distribution schemes for advection–diffusion problems on quadrilateral cells, Paper AIAA-2005-4990, 2005.
[22] T.J.R. Hughes, The Finite Element Method: Linear Static and Dynamic Finite Element Analysis, Dover, 2000.
[23] C. Hirsch, A general analysis of two-dimensional convection schemes, in: VKI LS 1991-01, 1991.
[24] S. Abarbanel, A. Kumar, Compact high-order schemes for the Euler equations, J. Sci. Comput. 3 (1988) 275–288.
[25] A. Lerat, C. Corre, Residual-based compact schemes for multidimensional hyperbolic systems of conservation laws, Comput. Fluids 31 (2002) 639–661.
[26] H. Nishikawa, P. Roe, On high-order fluctuation splitting schemes for Navier–Stokes equations, in: Proceedings of the Third International Conference on Computational Fluid Dynamics, ICCFD3, Toronto, July 2004.
[27] M.A. Christon, M.J. Martinez, T.E. Voth, Generalized Fourier analyses of the advection–diffusion equation—Part I: one-dimensional domains, Int. J. Numer. Methods Fluids 45 (2004) 839–887.
[28] T.E. Voth, M.J. Martinez, M.A. Christon, Generalized Fourier analyses of the advection–diffusion equation—Part II: two-dimensional domains, Int. J. Numer. Methods Fluids 45 (2004) 889–920.
[29] R.M. Smith, A.G. Hutton, The numerical treatment of advection: a performance comparison of current methods, Numer. Heat Transfer 5 (1982) 439–461.